Impact of Operating Parameters on Extended BWR Burnup Credit

Office of Nuclear Regulatory Research

Impact of Operating Parameters on Extended BWR Burnup Credit

Prepared by

Brian J. Ade
William (B. J.) Marshall
Germina Ilas
Benjamin R. Betzler
Stephen M. Bowman

Oak Ridge National Laboratory
Managed by UT-Battelle, LLC
Oak Ridge, TN 37831-6170

Office of Nuclear Regulatory Research

EXECUTIVE SUMMARY

Applicants for certificates of compliance for spent nuclear fuel (SNF) transportation and dry storage systems perform analyses to demonstrate that these systems are adequately subcritical per the requirements of Title 10 of the Code of Federal Regulations (10 CFR) Parts 71 and 72. For pressurized water reactor (PWR) SNF, these analyses may credit the reduction in assembly reactivity caused by depletion of fissile nuclides and buildup of neutron-absorbing nuclides during power operation. This credit for reactivity reduction during depletion is commonly referred to as *burnup credit* (BUC). US Nuclear Regulatory Commission (NRC) staff review BUC analyses according to the guidance in the *Division of Spent Fuel Storage and Transportation Interim Staff Guidance* (ISG) 8, Revision 3, *Burnup Credit in the Criticality Safety Analyses of PWR Spent Fuel in Transportation and Storage Casks*.

The technical basis for extended BWR BUC (beyond peak reactivity) is under evaluation in a research program being conducted by Oak Ridge National Laboratory (ORNL) under contract with the NRC Office of Research. NUREG/CR-7158 (*Review and Prioritization of Technical Issues Related to Burnup Credit for BWR Fuel)* identified and ranked parameters of importance to BWR BUC. NUREG/CR-7224 (*Axial Moderator Density Distributions, Control Blade Usage, and Axial Burnup Distributions for Extended BWR Burnup Credit*), summarizes impacts of the three highest-importance parameters: (1) axial coolant density distributions, (2) control blade usage, and (3) axial burnup profiles on extended BWR BUC.

NUREG/CR-7158 identified several other reactor operating parameters of medium importance that warranted in-depth analysis, such as fuel temperature, specific power, operating history, bypass water density, and the correlation of operating conditions. The impacts of these operating conditions are documented herein. The assessments were performed using a 10 × 10 GE14 fuel assembly model in the GBC-68 cask model that served as the reference configuration in previous studies. The assembly depletion, decay, and the cask criticality simulations were performed using the SCALE code system.

The fuel temperature, specific power, power history, and bypass water density were independently varied for the assembly depletion calculations, while all other parameters were held constant, to ascertain the individual impact of each of the varied parameters on cask reactivity. The results indicate that impacts of these four factors are small compared to the previously studied parameters of coolant density, control blade exposure, and burnup profile.

To study the importance of the correlation of operating parameters, base conditions that result in limiting cask reactivity estimates were selected for the assembly-specific conditions of interest (control blade usage, coolant density, axial burnup profile, and fuel temperature). Assembly-specific conditions were substituted for the base conditions to determine the impact of using assembly-specific (correlated) data for the control blade, coolant density, burnup profile, and fuel temperature. The results indicate that cask reactivity is reduced by using assembly-specific versus individually-limiting conditions, but the magnitude of this reduction is highly dependent on the chosen assembly and its specific conditions.

The results of these studies provide specific insight on the magnitude and direction that the changes in these considered operating parameters have on cask reactivity. The detailed data used in these studies were available from one source, and covered a single cycle of operation from a single plant, so specific recommendations on how to handle operating parameters within extended BUC analyses have not been made. Future work can be performed to demonstrate wider applicability of the conclusions drawn here if or when additional data become available.

CONTENTS

LIST OF FIGURES

LIST OF TABLES

x

ACRONYMS, ABBREVIATIONS, INITIALISMS, AND DEFINITIONS

1D   one-dimensional

2D   two-dimensional

3D   three-dimensional

actinide-only (AO) isotope set
> a limited set of isotopes that include only actinide elements and oxygen. (The isotopes in this set are listed in Table 2.1.)

actinide-plus-fission-product (AFP) isotope set
> a set of isotopes that is less limited than an actinide-only isotope set, including more actinide isotopes than the actinide-only set, some major fission product isotopes, and oxygen. (The isotopes in this set are listed in Table 2.1., originally from NUREG/CR-7108)

AFP   actinides and major fission products

AO   actinide only

assembly-specific conditions
> a set of operating conditions for that were experienced by a specific fuel assembly

assembly-specific conditions study
> a series of calculations used to determine the effect simulating assembly-specific operating conditions for the control blade history, coolant density profile, axial burnup profile versus using limiting, but uncorrelated data for these parameters.

axial coolant density study
> a series of calculations used to determine the effect of various axial coolant density distributions during depletion on the k_{eff} value of the SNF uniformly loaded in a storage and/or transportation system.

BA   burnable absorber

BOC   beginning of cycle

BOL   beginning of life

BUC   burnup credit

burnup   a measure of the energy produced by a fuel assembly or reactor per unit mass of initial heavy metal (in this report, initial uranium)

BWR   boiling water reactor

cask   a generic term for a storage and/or transportation system for fuel assemblies

CFR   Code of Federal Regulations

correlated parameters
assembly conditions that are correlated; used interchangeably with "assembly-specific conditions".

CSAS   SCALE's Criticality Safety Analysis Sequence

CV   case ID (**C**ontrol blade + **V**oid fraction = "**CV**") that uses assembly-specific conditions for the control blade history and coolant density (void fraction), while base conditions are used for the burnup profile and fuel temperature.

CVB   case ID (**C**ontrol blade + **V**oid fraction + **B**urnup profile = "**CVB**") that uses assembly-specific conditions for the control blade history, coolant density, and burnup profile, while the base fuel temperature is used.

CVBT   case ID (**C**ontrol blade + **V**oid fraction + **B**urnup profile + fuel **T**emperature = "**CVBT**") that uses assembly-specific conditions for all parameters being tested**.**

distributed burnup profile
generic term for any nonuniform axial representation of accumulated burnup in a fuel assembly

DOM   dominant or full fuel assembly lattice

end effect
the difference in calculated k_{eff} for an SNF system based on modeling a distributed burnup profile instead of a uniform burnup profile. A positive end effect indicates that the use of a distributed burnup profile results in a higher calculated k_{eff} value.

ENDF   evaluated nuclear data file

EOC   end of cycle

EOL   end of life

extended BWR BUC
crediting of reactivity reduction due to fuel depletion and, potentially, buildup of neutron-absorbing nuclides at burnups beyond peak reactivity burnup

GE   General Electric Company

GWd   gigawatt day

ISG   Interim Staff Guidance

KENO   SCALE's 3D Monte Carlo criticality transport module

limiting conditions/assumptions
assumptions which lead to higher k_{eff} values for the fuel contained in a storage or transportation system

LEU   low enriched uranium

MTHM   metric tons of heavy metal

MTU   metric tons of uranium; in LEU systems, MTU and MTHM are equivalent

MW   megawatt

MWd   megawatt day

NEWT   SCALE's 2D neutron transport solver used in the TRITON sequence

NRC   US Nuclear Regulatory Commission

OH   operating history

ORIGEN **O**ak **R**idge **I**sotope **GEN**eration; SCALE module used to simulate irradiation and decay of materials

ORNL   Oak Ridge National Laboratory

pcm   percent mille, equivalent to 10^{-5}

peak reactivity
a phenomenon in which the effective multiplication factor (k_{eff}) for an assembly or a 2D slice of the assembly is higher at some burnup than it is at BOL. This is a common feature of BWR assemblies and is caused by the depletion of the BA at a more rapid rate than depletion of the fuel.

peak reactivity analysis
a class of criticality safety methods used to demonstrate safe storage of fuel assemblies. These methods are discussed in some depth in NUREG/CR-7194.

PWR   pressurized water reactor

reactivity in this document, a term used interchangeably with k_{eff}, not meant in the strict technical sense of relative distance from the critical condition

relative burnup
the burnup of one assembly or region of an assembly in comparison to another assembly or region

relative reactivity
    reactivity of one assembly, region of an assembly, or model in comparison to another assembly, region, or model

SNF   spent nuclear fuel

TRITON   SCALE's arbitrary-geometry depletion sequence that automates cross-section processing, neutron transport, and depletion calculations for 1, 2, or 3D geometries.

uniform profile
    an axial profile that is a single, constant value over the entire axial length

VAN   vanished fuel assembly lattice

XSPROC   SCALE's cross section processing module

1   INTRODUCTION

Applicants for certificates of compliance for spent nuclear fuel (SNF) transportation and dry storage systems perform analyses to demonstrate that these systems are adequately subcritical per the requirements of Title 10 of the Code of Federal Regulations (10 CFR) Parts 71 and 72 [1]. For pressurized water reactor (PWR) SNF, these analyses may credit the reduction in assembly reactivity caused by depletion of fissile nuclides and buildup of neutron-absorbing nuclides during power operation. This credit for reactivity reduction during depletion is commonly referred to as *burnup credit* (BUC). US Nuclear Regulatory Commission (NRC) staff review BUC analyses according to the guidance in the *Division of Spent Fuel Storage and Transportation Interim Staff Guidance* (ISG) 8, Revision 3 [2], *Burnup Credit in the Criticality Safety Analyses of PWR Spent Fuel in Transportation and Storage Casks*.

BUC for boiling water reactor (BWR) SNF is not addressed in ISG-8. However, a technical basis for peak reactivity BWR BUC methods is provided in NUREG/CR-7194 [3]. Peak reactivity occurs when the effective multiplication factor (k_{eff}) for a lattice, or a two-dimensional (2D) axial slice of the assembly, reaches its highest value at some burnup beyond beginning of life (BOL). This is a common feature of BWR assemblies and is caused by depletion of the burnable absorber (BA) at a more rapid rate than depletion of the fuel. There is potential interest within the nuclear industry to extend BWR BUC to higher burnups beyond peak reactivity burnup. In this document, *extended BWR BUC* is defined as credit for the reduction in reactivity at burnups greater than the peak reactivity burnup. Studies assessing the impacts of axial coolant density distributions, control blade usage, and axial burnup profiles on extended BWR BUC are documented in NUREG/CR-7224 [4]. The impact of each of these phenomena was evaluated to identify limiting conditions and assumptions for use in extended BWR BUC analyses.

The analysis of the time-dependent nature of the axial coolant density in NUREG/CR-7224 indicated that use of cycle-averaged coolant density values (averaged in time, not in space) results in a relatively small bias that is less than 0.25% Δk_{eff}. The axial coolant density study highlighted the need to use a true axial coolant density profile, as the importance of the axial top portion of a spent BWR fuel assembly greatly outweighs the bottom and middle portions. Use of a uniform core-averaged coolant density profile (e.g., 40% void), or use of a graded profile constructed by averaging the coolant density in each axial node over multiple assemblies results in nonconservative SNF cask reactivity values. Limiting profiles with low coolant densities at the axial top of the fuel assembly can be constructed by selecting a limiting axial coolant density profile from available data, or they can be constructed by selecting the minimum density in each axial node from a collection of applicable actual profiles.

BWRs are operated using the control blades during operation as a means of reactivity control, so the usage of the control blades impacts SNF reactivity. Investigations to study the impact of control blade usage, documented in NUREG/CR-7224, indicated that control blade insertion of less than 50% into the core has almost no impact on cask reactivity. The control blade study indicated that the limiting conditions are those that result in the control blade being inserted deeply into the core for long periods of time, and especially near the end of life. Although unrealistic, full- or near full-depth control blade insertion for the entire irradiation results in increases in cask reactivity of 4.0–4.5% Δk_{eff} compared to no control blade insertion. Based on the study of realistic control blade histories, a reactivity penalty of 0.6–1.2% Δk_{eff} (as compared to no control blade insertion) may be sufficient to cover possible operating histories.

As indicated in NUREG/CR-7224, the effect of axial burnup profiles on BWR SNF is significant. The range of cask k_{eff} values resulting from the profiles used in that study was as large as 7.6% Δk_{eff}. Low burnup near the top end of the fuel assembly results in a significant end effect, leading to high cask k_{eff} sensitivity to the selected burnup profile. Distributed burnup profiles rather than uniform burnup profiles should be used for analysis, as end effects up to 12.7% Δk_{eff} were observed.

NUREG/CR-7158 [5], *Review and Prioritization of Technical Issues Related to Burnup Credit for BWR Fuel,* indicates that the topics studied in NUREG/CR-7224 (axial coolant density profile, control blade history, and burnup profile) are of high importance. NUREG/CR-7158 indicates that there are several other parameters of importance to BWR BUC, including fuel temperature, operating history, specific power, and bypass water density. A summary of the effect of each of these parameters is provided in Section 3.

NUREG/CR-7158 also indicates that the correlation of various operating parameters, i.e. conditions that are experienced by an individual assembly, warrant further study. Because BWRs use control blades during operation, there can be significant changes to the local axial power shape, coolant density profile, and other parameters when the blades are inserted. Previous studies [4] separately examined the reactor operating parameters that impact fuel cask reactivity. The previous studies identified limiting conditions for fuel cask reactivity or the direction of trends with cask reactivity (e.g., lower coolant densities result in higher cask reactivity). However, simultaneously using limiting conditions for all parameters may be unrealistic. When the control blades are inserted deeply into the reactor (a limiting condition), the power is reduced, and the void fraction decreases (a less limiting condition). The study documented in Section 4 identifies the impacts of using assembly-specific conditions for the control blade history, coolant density profile, burnup profile, and fuel temperature profile. Cask reactivity is reduced by using assembly-specific operating conditions versus combining limiting conditions for the individual parameters of interest, but the magnitude of the reactivity reduction varies based on each assembly and its operating conditions.

Finally, Section 5 provides a summary of the present studies within the context of the previous studies cited above. The conclusions summarize the technical basis for extended BWR burnup credit as a result of the past and present studies.

2 CODES, METHODS, AND MODELS

2.1 Codes and Methods

The analyses documented in this report were performed using a series of codes and models to simulate the fuel assembly irradiation and the SNF reactivity in an SNF storage or transportation cask. The codes, associated data, and models used are summarized in this section. The assembly and cask configurations used in these studies are consistent with those used in NUREG/CR-7224 [4].

The computational procedure included the following main steps:

1. Conduct depletion simulation to determine the isotopic composition of the irradiated fuel assembly at its discharge from the reactor.

2. Conduct decay simulation of the discharged assembly's isotopic composition to determine the nuclides present at five years of cooling time after discharge from the reactor.

3. Perform a criticality calculation for the GBC-68 cask to determine the effective multiplication constant (k_{eff}) using the isotopic composition of the SNF obtained in step 2.

These computational steps and the SCALE modules and codes involved are illustrated in Figure 2.1 and are further described in this section. Version 6.2.1 of the SCALE code system [6] was used for all calculations in this work.
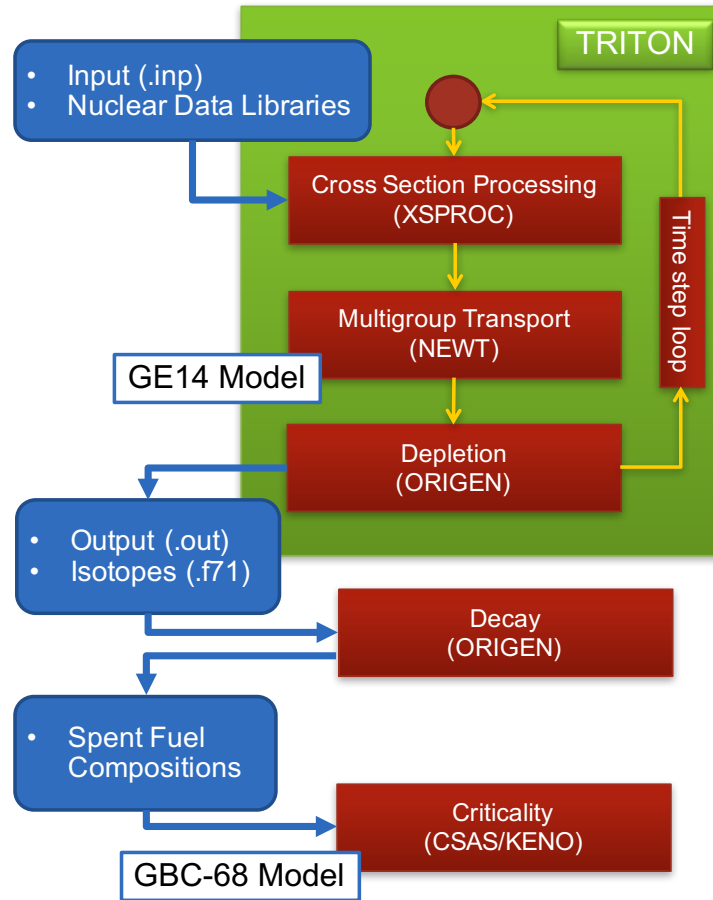
Figure 2.1.   SCALE sequences and modules used for depletion and criticality calculations in this report.

2.1.1   TRITON

TRITON is a multipurpose SCALE control module for neutron transport, depletion, and sensitivity and uncertainty analysis [8,9]. In this work, the TRITON *t-depl* sequence was used to simulate the assembly depletion history via a series of coupled neutron transport and depletion calculations. As illustrated in Figure 2.1, the TRITON flow chart includes automated, problem-dependent cross section processing (XSPROC), multigroup deterministic neutron transport (NEWT), and depletion (ORIGEN) calculations over a series of time steps to cover the assembly irradiation history from the onset of its irradiation to the time of its discharge from reactor.

Through a joint NRC and Oak Ridge National Laboratory (ORNL) project, the ORNL BWR BUC project gained access to proprietary operating data for a single cycle of a BWR core. The data include inlet and outlet conditions and traveling in-core probe (TIP) data, as well as simulated core-follow data for every fuel assembly in the reactor. The data were obtained from a recent cycle that contained four different modern BWR fuel assembly design types. Each fuel assembly has been modeled with 25 different axial nodes, and the 690-day cycle was simulated using more than 240 time steps. The size of the time steps varies slightly, but all steps are less than 5 effective full power days in length. State variables needed for the studies documented here were extracted from the simulated data.

TRITON two-dimensional (2D) simulations were performed for each axial slice (node) defined in the core-follow simulations [4] from which the assembly design and operating data were taken (25 nodes in total). For consistency, the same basic modeling assumptions and options that were used in previous calculations [4] were also used in the TRITON calculations for this work, as summarized below:

- The transport model includes a set of 94 nuclides corresponding to the "addnux=2" option (default in TRITON), while more than 2,000 nuclides are tracked by the ORIGEN depletion and decay calculations.
- The gadolinium-bearing fuel rods in the assembly are modeled with seven equal-area radial rings to accurately capture the radial dependence of the gadolinium depletion [8].
- The 252-group ENDF/B-VII.1 neutron cross section library is used for neutron transport with the NEWT code.
- The detailed power history is modeled in the TRITON calculations by directly specifying the power in the TRITON depletion specification. The timetable block, which is used extensively in the TRITON calculations, modifies properties of selected materials in the model during depletion. In this work, the timetable block is used to adjust coolant densities, fuel temperatures, and the presence or absence of the control blade during depletion calculations.

2.1.2 ORIGEN

ORIGEN is the depletion and decay simulation code in SCALE used to determine time-dependent nuclide concentrations, activities, and radiation source terms for more than 2,000 isotopes involved in transmutation, fission, and radioactive decay processes [9]. In addition to its use in this work as part of the TRITON depletion sequence, ORIGEN is also used to perform standalone radioactive decay simulations to determine the change in isotopic composition of the assembly's fuel after its discharge from the reactor. The decay library used with ORIGEN is based on ENDF/B-VII.1 data [10].

2.1.3 KENO

The Criticality Safety Analysis Sequence (CSAS)/KENO is used to perform reactivity calculations for the GBC-68 cask model. The sequence provides automated problem-dependent cross section processing followed by 3D multigroup Monte Carlo neutron transport calculations to solve the k_{eff} eigenvalue problem. All calculations are performed using the transport code KENO V.a and the 252-group neutron cross section library based on ENDF/B-VII.1 data.

Two sets of nuclides are used for fuel modeling in the CSAS models: (1) major actinides only (AO), and (2) major and minor actinides and major fission products (AFP). The nuclides used in the AO and AFP nuclide sets are taken from NUREG/CR-7109 [11] and are the same as those typically used when performing PWR BUC calculations. The same isotope sets are used for BWR BUC studies because the same nuclides result from fission in both PWR and BWR types of light water reactors. Table 2.1 provides the BUC nuclides considered in the AO and AFP sets.

Table 2.1.   Isotopes included in the AO and AFP isotope sets

10 AO isotopes									
^{234}U	^{235}U	^{238}U	^{238}Pu	^{239}Pu	^{240}Pu	^{241}Pu	^{242}Pu	^{241}Am	^{16}O

29 AFP Isotopes									
^{234}U	^{235}U	^{236}U	^{238}U	^{237}Np	^{238}Pu	^{239}Pu	^{240}Pu	^{241}Pu	^{242}Pu
^{241}Am	^{243}Am	^{95}Mo	^{99}Tc	^{101}Ru	^{103}Rh	^{109}Ag	^{133}Cs	^{147}Sm	^{149}Sm
^{150}Sm	^{151}Sm	^{152}Sm	^{143}Nd	^{145}Nd	^{151}Eu	^{153}Eu	^{155}Gd	^{16}O	

2.2   Models

2.2.1   GBC-68 Cask

The GBC-68 computational benchmark model was developed in NUREG/CR-7157 [12] as a generic BUC cask for modeling BWR SNF. The KENO model of the fuel loaded in the cask explicitly represents each fuel rod, including its gap and cladding in the General Electric Company (GE)14 fuel assemblies. Part-length rods are truncated at the appropriate elevation so that both the full lattice (referred to as *full* or *dominant* and abbreviated as "DOM") and the vanished lattice (VAN) are included explicitly in the KENO model. Section 2.2.2 includes further discussion of the GE14 assembly modeling. The fuel assembly channel model is simplified in KENO and is represented with constant thickness and squared corners. All fuel assemblies in the GBC-68 cask model are assumed to contain fuel with identical compositions and irradiation histories. KENO calculations performed with depleted fuel compositions generated by TRITON and ORIGEN assume a single average composition for fuel without gadolinium, as well as seven unique compositions for the rings modeling the gadolinium fuel pins in each axial node.

All KENO models contain 25 axial nodes, each 6 inches in length (15.24 cm). Figure 2.2 shows a radial view of the GBC-68 half-cask model depicting the cask body, basket, and fuel assemblies. Figure 2.3 shows an axial view of the model with each unique axial fuel composition shown in a different color.
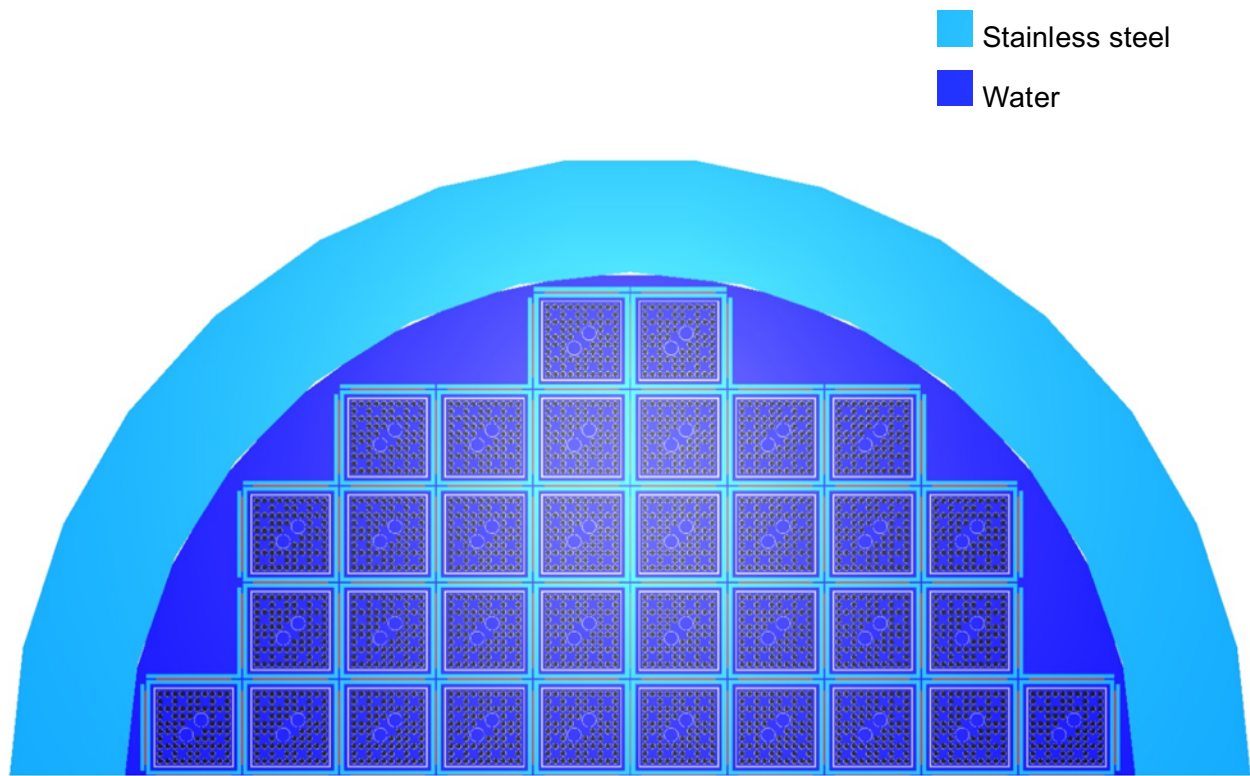
Figure 2.2.   Radial view of the GBC-68 cask model in KENO in the VAN lattice.
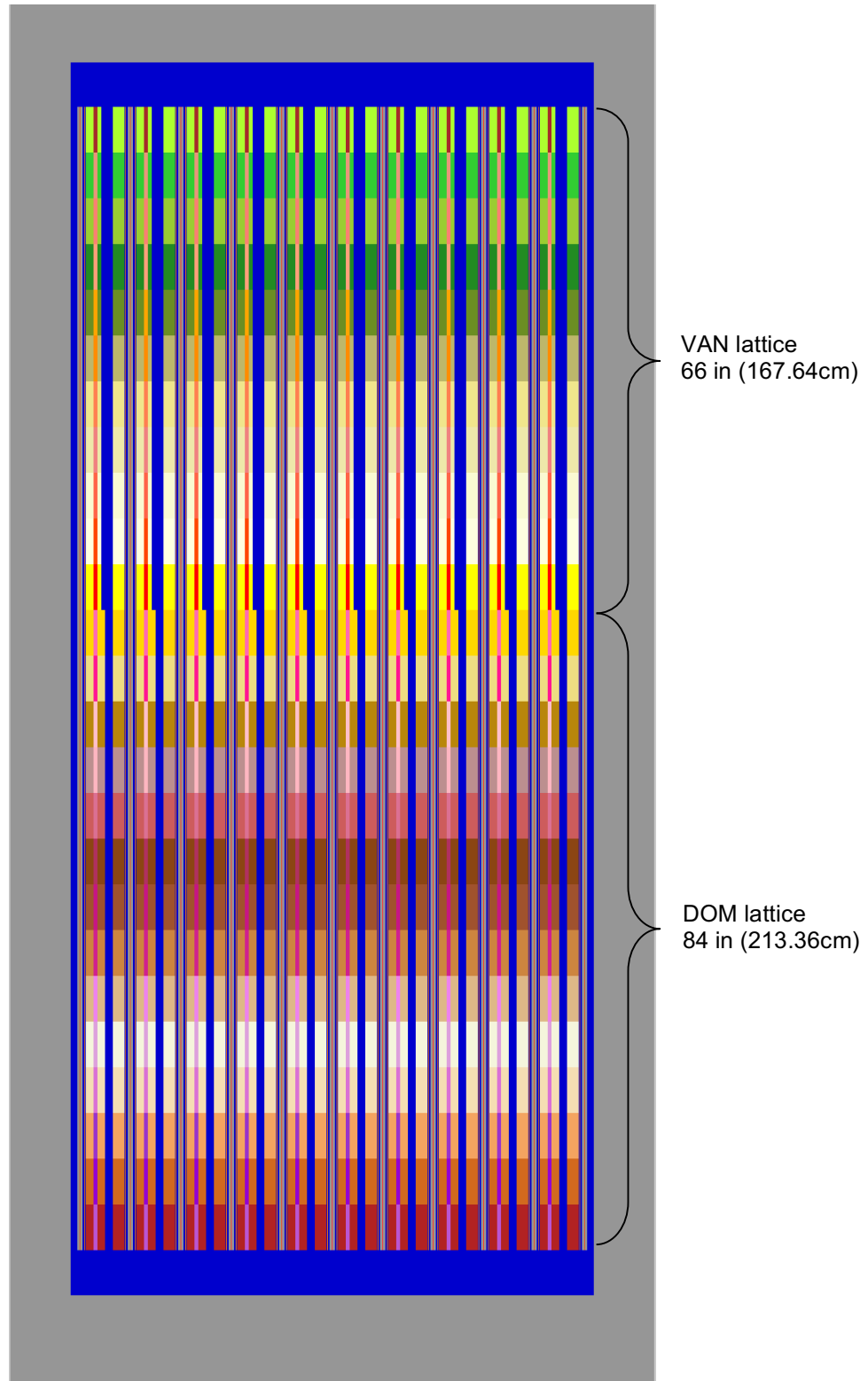
Figure 2.3.   Axial view of GBC-68 cask KENO model.

2.2.2 GE14

GE14 is the only fuel assembly design used in these studies. This assembly has a 10 × 10 array of fuel pins and contains two large central water rods, each of which displaces four fuel rods. The GE14 fuel assembly can contain many axial levels with varying fuel enrichment and gadolinium loading. Due to the presence of part-length fuel rods which terminate at approximately half the total height of the fuel assembly, the GE14 fuel assembly contains two primary axial levels which are known as *zones*. These two axial zones are the DOM (dominant) and the VAN (vanished) lattices. A 2D slice through one of these axial zones is referred to as a *lattice*. The DOM lattice has fuel rods occupying every position in the fuel pin array. The vanished lattice is located axially above the part-length rods, so these rods are in effect removed or vanished from the lattice. TRITON representations of the DOM and VAN lattices are shown in Figure 2.4. All gadolinium-bearing rods contain the same absorber loading in both the DOM and VAN lattices. Two-dimensional representations of the two lattices in the KENO model of GBC-68 are shown in Figure 2.5. Axial enrichment zoning is not modeled for any calculations presented in this report, rather, a single enrichment of 4.5 wt% ^{235}U is used throughout the entire axial length of the fuel assembly.

(a)   (b)
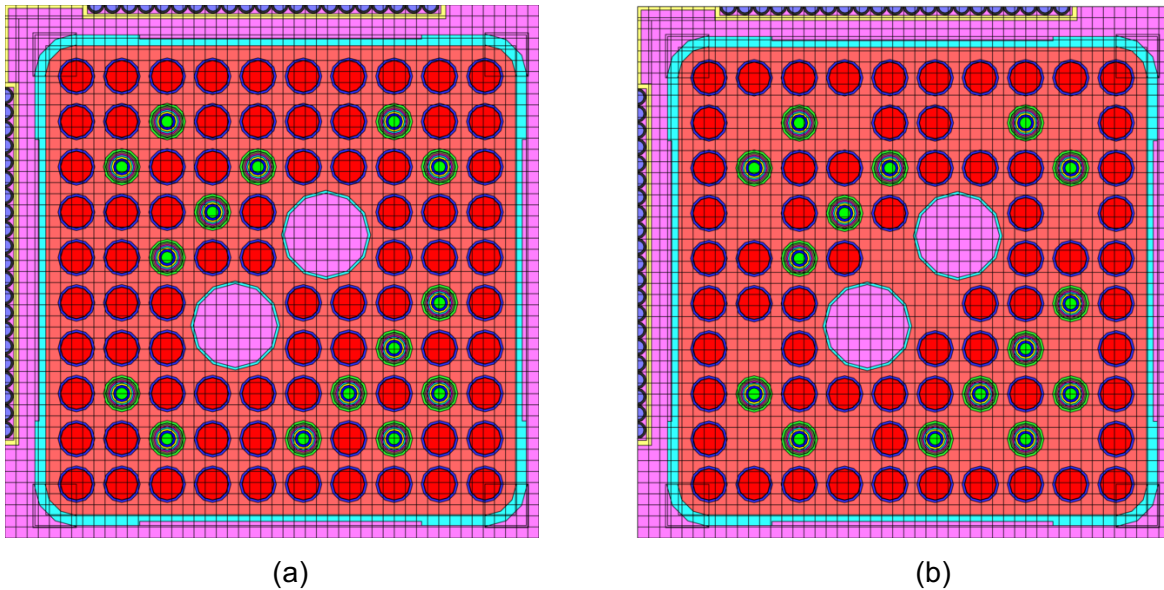
Figure 2.4.   TRITON model of the (a) DOM and (b) VAN lattice.
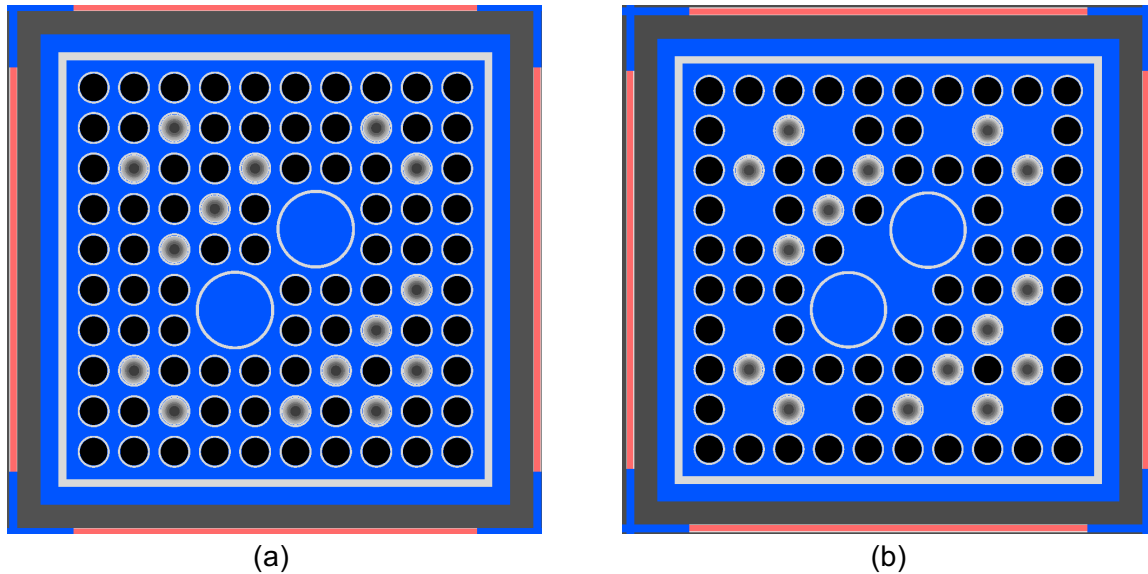
Figure 2.5.   (a) DOM lattice and (b) VAN lattice, both in storage cell in GBC-68.

The GE14 fuel assembly was chosen for the studies herein, as it is the most common fuel assembly type used in current US BWRs. The GE14 fuel assembly contains advanced geometry features commonly seen in modern BWR fuel assemblies (e.g., water rods, part-length rods). It is commonly loaded with pins enriched to near 5.0 wt % ^{235}U, and it typically contains many gadolinium-bearing fuel pins. Results from studying various characteristics in a modern, highly heterogeneous fuel lattice such as the GE14 can be potentially extended to other highly heterogeneous fuel configurations. A previous study [5] has shown that the GE14 assembly design is more reactive than smaller GE lattices (7 × 7, 8 × 8, and 9 × 9) for most burnups. Other lattice sizes may be more reactive at high burnup [5], but coolant density distribution, control blade history, axial burnup profile, and other effects examined herein are expected to be largely independent of assembly lattice size.

The fuel assembly design used in these studies is based on an actual assembly from the detailed core-follow data described in Section 3 of Ref. 4. All TRITON depletion calculations used 4.5 wt % ^{235}U in all pins, and they used 15 gadolinium-bearing rods with 7 wt % Gd_2O_3. This single assembly design is used throughout the calculations to assess the important effects of operating parameters and assembly-specific conditions independent of any effects that may have been caused by differing fuel or absorber loadings. Additional enrichments, gadolinium loadings, or gadolinium-bearing pin patterns are not considered in this report, but were previously analyzed [3]. The items examined in this report are not expected to have a significant sensitivity to differing fuel loadings or loading patterns.

3 IMPACT OF OPERATING PARAMETERS ON CASK REACTIVITY

3.1 Background

Previous review and prioritization of technical issues related to BUC for BWR SNF [5] resulted in identifying phenomena and parameters important to BWR BUC methodology and providing recommendations for further BWR BUC research. Three of the research objectives categorized as high priorities were (1) identification and use of axial burnup profiles, (2) treatment of axial coolant density profile, and (3) treatment of control blade usage during depletion. These three topics have been investigated and were documented [4]. Another priority recommendation [5] for BWR BUC, categorized as *medium impact*, consisted of investigation of reactor operating parameters in fuel depletion calculations. Fuel temperature, specific power, and bypass water density were listed as candidates for future studies. These three latter parameters are included, along with operating history, in the studies discussed in this section of the report.

To study these parameters, some basic assumptions are required. As previously stated, the GE14 fuel assembly and the GBC-68 SNF cask model have been used for all calculations. The axial void fraction profile and axial burnup profile were assumed to be the same as those used in NUREG/CR-7224 [4] and are shown in Figure 3.1. Actual nodal average burnup values are given in Figure 3.1, which are used directly in the studies in this section as no burnup variation is considered (assembly average burnup = 45.2 GWd/MTHM). Previous studies [4] and the assembly-specific conditions study documented in Section 4, conserve the shape of the burnup profile but scale the values to facilitate comparison to other burnup profiles.

(a) Void fraction profile   (b) Burnup profile
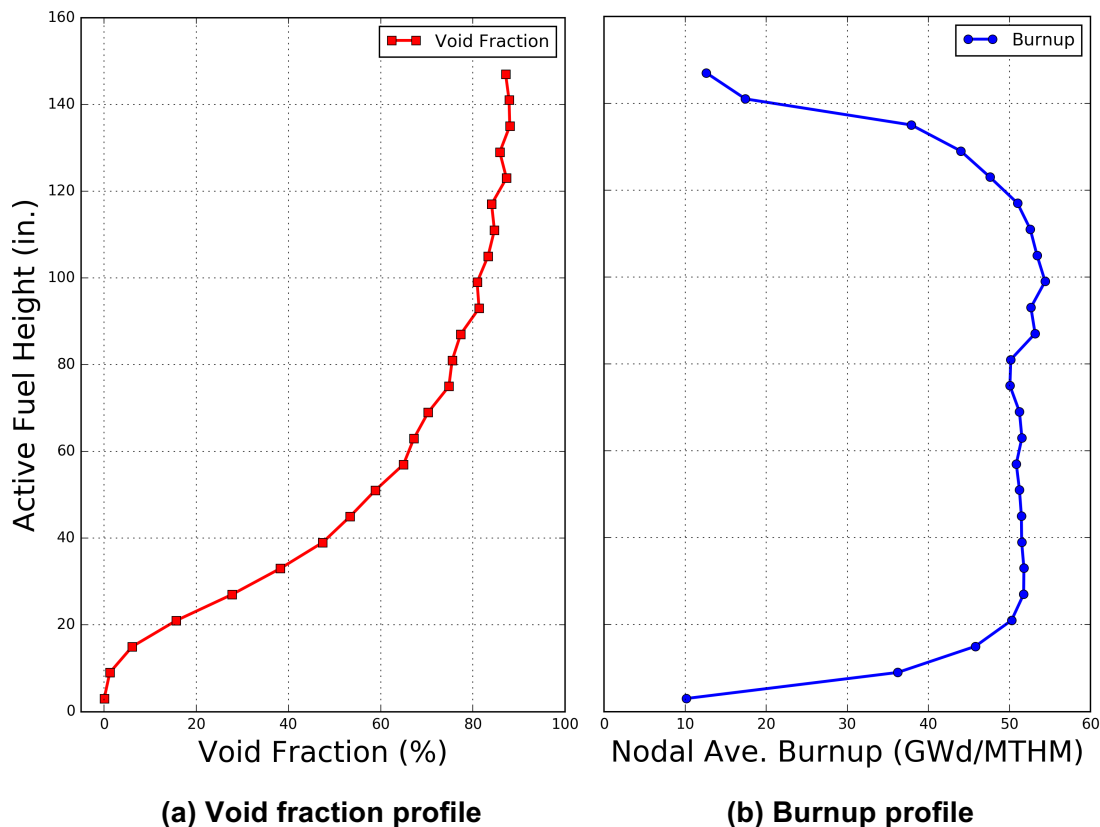
Figure 3.1. **(a) Axial coolant void profile and (b) axial burnup profile.**

3.2   Description of Studies

3.2.1   Fuel Temperature

The main fuel temperature study is meant to determine the sensitivity of fuel cask reactivity to changes in fuel temperature. To determine if axially-uniform or axially-profiled fuel temperatures should be used in this primary study, a limited analysis of the effect of the axial fuel temperature profile was conducted. The results of this study indicated that the sensitivity of cask reactivity to the fuel temperature profile (i.e. axial shape) is very small (less than 0.1% Δk_{eff}). As a result, the fuel temperature study documented in this section uses a single fuel temperature in all fuel rods, with no axial or radial variation.

Nine values are used for the fuel temperature sensitivity studies, covering a range from 596.1 to 1,296.1 K in 100 K increments. A nodal fuel temperature of 796.1 K was reported as the core- and cycle-averaged temperature over all fuel assemblies in the available core-follow data for a BWR core's single cycle [4]. This temperature was used as the nominal value for previous studies conducted in this project [3,4] and was used as a basis for selecting the fuel temperatures in this study.

The range used for the fuel temperature in this work includes the range of temperatures available for all assemblies in the core-follow data at all time steps in the cycle [4]. The overall maximum nodal fuel temperature in the core-follow data is less than 1,100 K at any time point during the cycle. However, to cover higher temperatures that may occur during operation [13] and to ensure consistency with data used previously in similar BWR studies [5,14], the range was extended to ~1,300 K.

Increased fuel temperature during BWR depletion calculations leads to increased production of actinides important to BUC (^{239}Pu, in particular) [5,14], and consequently, it leads to an increase in cask reactivity. This effect is primarily due to the change in the neutronic environment by resonance Doppler broadening of ^{238}U cross sections with increasing temperature that leads to increased ^{239}Pu production.

The distributions of the fuel temperatures for the core-follow data in all 624 assemblies at beginning of cycle (BOC) and end of cycle (EOC) are illustrated in Figure 3.2. In this context, BOC and EOC correspond to the first and last full-power steps in the cycle. The cycle- and core-average fuel temperature profile is plotted as a bold black line. The atypical shapes in the BOC fuel temperature distributions are due to the presence of control blades inserted directly adjacent to those fuel assemblies.
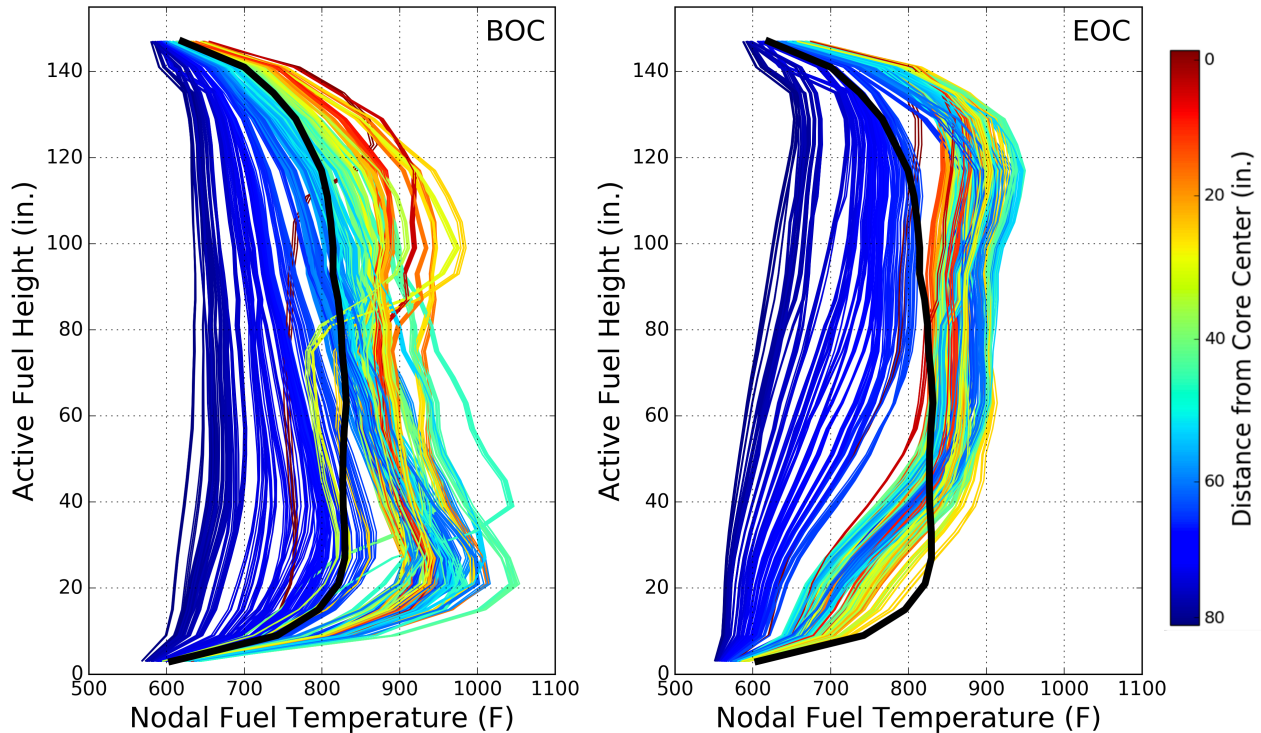
Figure 3.2. **Fuel temperature distributions for all assemblies at BOC (left) and EOC (right). The bold black line represents the core-average fuel temperature profile.**

3.2.2   Bypass Water Density

Consistent with NUREG/CR-7224, the nominal value of the bypass water density for the cycle of operation studied is 0.73549 g/cm^3, which corresponds to the subcooled water circulated outside of the assembly channel and within the two large water rods in the assembly. This bypass water is shown with the pink color in the illustration of the assembly configuration (see Figure 2.4). No relevant published data were found regarding the axial shape or the range of bypass water density variations that may occur under normal BWR operation. For that reason, no axial variation is considered for this study. To quantify the impact due to changes in the bypass density during operation, the sensitivity study discussed here considered a range of values between the nominal density and 10% less than the nominal density.

For sensitivity studies in this work, 11 values were used for the bypass water density to cover a range from nominal to a 10% density reduction in 1% increments. A decrease in bypass water density will cause hardening of the neutron spectrum and consequently an increase in plutonium production, and it will also affect the production of other actinides and fission products sensitive to changes in neutron spectrum. The magnitude of this effect will depend on the magnitude of the change in water density. As previously stated, published data quantifying the actual range of bypass density values was not found, however, a 10% reduction in bypass density is expected to bound the variation in bypass density for normal operation.

3.2.3   Specific Power

The assembly depletion simulations in this report account for the axial variation of the assembly burnup, which is illustrated in Figure 3.1. Given the linear relationship between specific power

13

(MW/MTHM) and burnup (MWd/MTHM) for the assembly, the specific power axial profile averaged over life and the burnup axial profile at discharge are the same shape (i.e., the normalized axial distribution is the same). This study is meant to determine the cask reactivity sensitivity to changes in the specific power independent of the shape of the burnup profile and independent of the power history. In other words, this study is designed to determine the cask reactivity sensitivity to the rate at which the assembly reaches a certain burnup value.

To achieve this, the specific power sensitivity study considered 90% and 110% specific power variations relative to then nominal power. The same relative power distribution is used in all three cases: (1) nominal, (2) 90% of nominal, and (3) 110% of nominal. However, the specific power in a given node is adjusted to correspond to 100%, 90%, or 110% relative to its value for the nominal case. The same number of depletion steps is used in each of the three cases. Because the assembly burnup at discharge is the same in these three cases, the change in specific power requires the change in the total irradiation time to conserve the burnup. For the nominal case [4], the total irradiation time is 2,070 days (690 days per cycle × 3 cycles). For cases with specific power at 90% relative to nominal, the total irradiation time is 2,300 days, and for cases with specific power at 110% relative to nominal, the total irradiation time is 1,882 days. Derivation of the irradiation times for each of the three cases is described by the equation shown below:

$$p_0 t_0 = k p_0 t_1 \Rightarrow t_1 = \frac{t_0}{k},$$

where p_0 and t_0 are the specific power and irradiation time for the nominal case, k is the specific power multiplier (0.9 or 1.1) for the perturbed case, and t_1 is the irradiation time for the perturbed case.

3.2.4   Operating History

In the context of BUC applications, the term *operating history* usually refers to cycle length, downtime between cycles, and power level for each cycle. The operating history scenarios investigated in this study (described in Table 3.1) are used to assess the effect of the power level and downtime for a given assembly burnup at discharge. Detailed analysis of the effect of the burnup profile is provided in NUREG/CR-7224 [4]. This study is meant only to determine the cask reactivity sensitivity to variation of power and downtime throughout the irradiation history.

Nominal conditions for the axial coolant density and axial burnup profile (Figure 3.1) are used for all assembly modeling parameters for the ten operating histories under consideration. Only assembly power history is varied for operating scenarios OH-1 through OH-10—the total discharge burnup for each case is the same. The power level per irradiation cycle (and equivalently the cycle burnup) and the decay time between irradiation cycles are varied so that the sum of the total burnup at EOL is the same for all case. I.e., in Table 3.1, the average of the power of the three cycles is 100%, resulting in equivalent burnup for all cases. OH-1 through OH-9 were constructed based on engineering judgement, while the OH-10 operating scenario was derived from available cycle-follow data and is discussed in detail at the end of this section.

Histories OH-1 through OH-3 are used to assess the impact of downtimes between cycles. Specific power is the same in each of the three cycles for these histories. History OH-1 represents continuous operation at full power with no downtime and is used as a baseline for comparison in this section. History OH-1 was used for all other sensitivity studies discussed in Section 3.2. History OH-2, which uses typical 30-day downtimes, is intended to assess the effect of using typical downtime versus excluding any downtime between cycles. History OH-3 is used to assess the impact of long downtime (720 days in this case) preceding the last irradiation cycle of an assembly before its discharge. One example of this scenario is an assembly that is

14

moved to a storage pool after two irradiation cycles, stored in the pool for approximately two years, and then irradiated for a third cycle before being finally discharged.

Histories OH-4 through OH-7 are used to assess the effect of power variation across the three cycles when all the following factors are the same: (1) downtime between cycles, (2) assembly burnup at discharge from the reactor, and (3) average power over the assembly's three cycles of irradiation (sum of % power values in Table 3.1 is 300%). Histories OH-4, OH-5, and OH-6 (highest power in first or second cycle, lowest power in third cycle) are considered representative of typical operation for most assemblies, whereas OH-7 (highest power in third cycle) is considered atypical. Scenarios with the highest power in the second cycle are possible for a fuel assembly with heavy initial gadolinium poison loadings that are depleted during the first cycle.

Histories OH-8 and OH-9 are used to test the effect of long downtime before the last irradiation cycle for a typical and an atypical power history. Except for the 720-day downtime before the third irradiation cycle, OH-8 and OH-9 are similar to OH-5 and OH-7, respectively. History OH-10 is similar to OH-4 (highest power in first cycle, lowest power in third cycle), but the power in the first two cycles is increased, while the third cycle power is significantly decreased. The construction of OH-10 is discussed in Sect. 3.2.4.1. All cases summarized in Table 3.1 are decayed for five years after irradiation.

Table 3.1.   Operating history scenarios

History	Cycle 1		Cycle 2		Cycle 3
	% power	downtime (d)	% power	downtime (d)	% power
OH-1	100	0	100	0	100
OH-2	100	30	100	30	100
OH-3	100	30	100	720	100
OH-4	120	30	100	30	80
OH-5	120	30	120	30	60
OH-6	100	30	120	30	80
OH-7	80	30	100	30	120
OH-8	120	30	120	720	60
OH-9	80	30	100	720	120
OH-10	136.15	30	116.53	30	47.33

3.2.4.1 Realistic Operating Power History Based on Core-Follow Data

The available core-follow data [4] used for various operating conditions cover only one cycle of operation. Therefore, the available data do not follow the full operating history for any given assembly from its first to its last irradiation cycle in the reactor. Based on the available one-cycle data, a realistic assembly operating history—identified as OH-10 in Table 3.1—was derived and applied to a three-cycle irradiation simulation. Derivation of this operating history is described in this section.

The core-follow data include information about the burnup history as a function of irradiation time for each axial node of each of the 624 assemblies in the core. The burnup distributions at EOC for the first-, second-, and third-cycle fuel assemblies are illustrated in Figure 3.3. This figure shows the active fuel height on the y-axis and the node burnup on the x-axis for all assemblies; the thick black dashed line on these plots represents the average axial EOC burnup distribution for that set of fuel assemblies. Similar to Figure 3.2, the EOC axial burnup profiles

plotted in Figure 3.3 are colored based on their location within the core—assemblies near the center of the core are colored in red and assemblies near the core periphery are colored in blue.

First-cycle fuel assemblies are easily identified by having zero burnup at BOC. There are 252 first-cycle assemblies in the core. On average, the burnup gain over one cycle for the first-cycle assemblies is 21.87 GWd/MTHM. Assemblies in the core with an average burnup at BOC of less than 25.5 GWd/MTHM (excluding zero burnup at BOC) are assumed to have undergone one cycle of irradiation and are considered second-cycle assemblies. There are 256 assemblies that meet this criterion; their burnup characteristics are listed in Table 3.2. On average, the burnup gain over the cycle for the second-cycle assemblies is 18.72 GWd/MTHM. The 116 assemblies in the core that are not first- or second-cycle assemblies are considered third-cycle assemblies. On average, the burnup gain over a cycle for these assemblies is 7.61 GWd/MTHM.

Some of the assemblies categorized as third-cycle assemblies may have experienced two, three, or more irradiation cycles prior to the cycle for which detailed core-follow data are available. These assemblies are categorized as third-cycle assemblies to enable a consistent comparison with the other operating history scenarios listed in Table 3.1, which all consider three cycles of irradiation.

Based on the assumptions and derivation discussed in this section, a derived typical core three-cycle irradiation history has a first-cycle burnup gain of 21.87 GWd/MTHM, a second-cycle burnup gain of 18.72 GWd/MTHM, and a third-cycle burnup gain of 7.61 GWd/MTHM, as well as a discharge burnup of 48.19 GWd/MTHM. Therefore, the burnup gain for each cycle relative to the discharge burnup is 45.38% for the first cycle, 38.84% for the second cycle, and 15.77% for the third cycle. Assuming each cycle of irradiation has the same cycle length, the power level per cycle relative to the average over all three cycles would be 136.15% for the first cycle, 116.53% for the second cycle, and 47.33% for the third cycle. The depletion simulation for history OH-10 was constructed using these percentages and the same assembly average burnup at discharge as histories OH-1 through OH-9—45.2 GWd/MTHM.

Table 3.2.   Burnup characteristics derived from core-follow data

	Burnup (GWD/MTHM)	First-cycle assemblies	Second-cycle assemblies	Third-cycle assemblies
	Minimum	0	15.59	27.71
BOC	Maximum	0	25.27	41.88
	Mean	0	21.50	35.93
	Minimum	16.62	34.44	37.44
EOC	Maximum	24.58	44.85	48.44
	Mean	21.87	40.22	43.53
	Cycle burnup[a]	21.87	18.72	7.61
	Burnup per cycle[b] (%)	45.38	38.84	15.77
	Power level per cycle[c] (%)	136.15	116.53	47.33

[a] Cycle burnup was calculated as $B_{cyc} = \frac{1}{N_{cyc}} \sum_{i=1}^{N_{cyc}} (B_i^{EOC} - B_i^{BOC})$, where i is index of assemblies in category cyc=1st, 2nd, or 3rd ; B is burnup; and N_{cyc} is the total number of assemblies in category cyc

[b] Burnup gain per cycle relative to discharge burnup (100%)

[c] Relative to average over all three cycles (sum over three cycles is 300% - number of cycles times 100%)
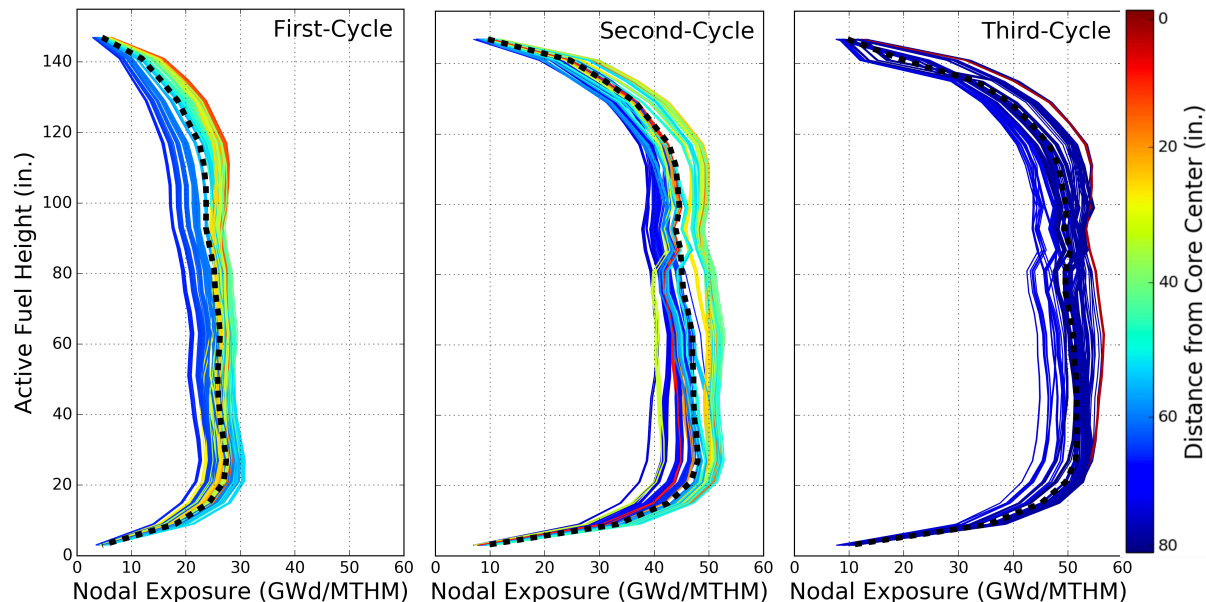
Figure 3.3.   Burnup distribution at EOC for first-, second-, and third-cycle fuel assemblies.

3.2.4.2 Operating Power Histories from Other Sources

Detailed operating power history data are rare in publicly available references, and where available, they generally involve older assembly designs and operating cycles [15]. A literature search was performed to identify sources of detailed operating histories for assemblies irradiated for three reactor cycles, to use in consistent comparison with the operating histories OH-1 through OH-9 (Table 3.1). Although this literature search was largely unsuccessful, some resulting information is briefly summarized here and is deemed as potentially valuable for understanding operating data in the context of future burnup credit applications for BWR spent fuel.

Cycle-by-cycle assembly burnup data are available for 60 GE 7 × 7 assemblies irradiated in the Cooper and Monticello BWRs operated in the United States [15]. These assemblies were irradiated in the reactor from Cycle 1. Two of the assemblies were only irradiated during Cycles 1 and 2, but the remaining assemblies were irradiated for 4, 5, or 6 cycles operated during 1974–1982 for Cooper and 1971–1975 for Monticello. Given the old design, data for these assemblies are not typical of the majority of BWR assemblies now in storage, and they also differ from those now in operation.

Cycle-by-cycle assembly burnup data are available for 23 BWR assemblies irradiated at various times between 1978 and 1992 in six different Swedish reactors [15]. These assemblies have unique designs: 8 × 8, 9 × 9, SVEA-64, and SVEA-100. They have been irradiated for 4 to 8 cycles in the reactor, with most of them irradiated for more than 5 cycles. The power levels for the last irradiation cycles vary widely among these assemblies, depending on the assembly and reactor, ranging between 36% and 119% of the lifetime-averaged power.

Power history data of a GE14 assembly [16] irradiated between 2000 and 2005 in the Swedish Forsmark 3 reactor is illustrated in Figure 3.4. This assembly was irradiated for five cycles and had a power level of 53% during the last cycle.

17
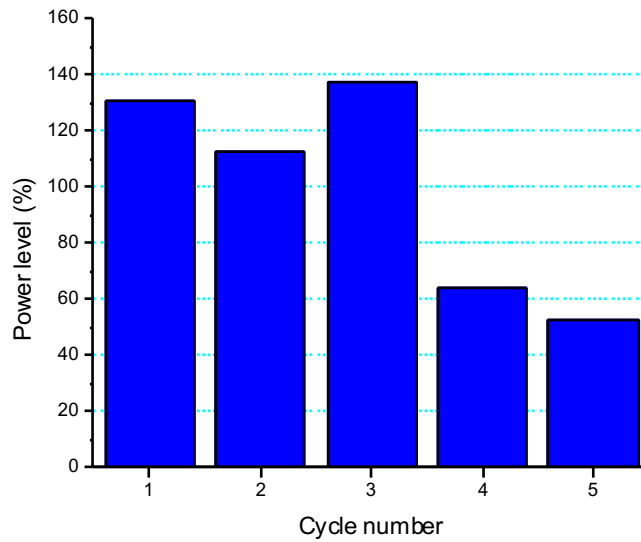
Figure 3.4.   Power history for Forsmark 3 assembly.

The number of irradiation cycles for the BWR assemblies in the US GC-859 database [17] discharged from the reactor between 1969 and 2013 [18] is illustrated in Figure 3.5. This plot shows the number of assemblies as a function of the number of cycles for which they were irradiated in the reactor. This is illustrated for four assembly types (7 × 7, 8 × 8, 9 × 9, and 10 × 10). The bar-style plot is color-coded to indicate the years of assembly discharge between 1969 and 2013. The most common number of cycles is three, while some fuel assemblies were irradiated for four or five cycles. However, the discharge burnup is the key parameter for burnup credit, not the total number of cycles. The results obtained for the assumed three-cycle history in this study would apply to a large extent to other multi-cycle histories if the discharge burnup is similar. While it is common to operate BWRs with fuel assemblies inserted for more than three cycles, the cycle length in this case would be shorter to maintain similar assembly discharge burnup values. As will be shown in the results to this study, there is very little impact to cask reactivity for varying the operating history (power level per cycle and downtime), so adding additional cycles that result in the same total discharge burnup will not result in significant changes to cask reactivity.
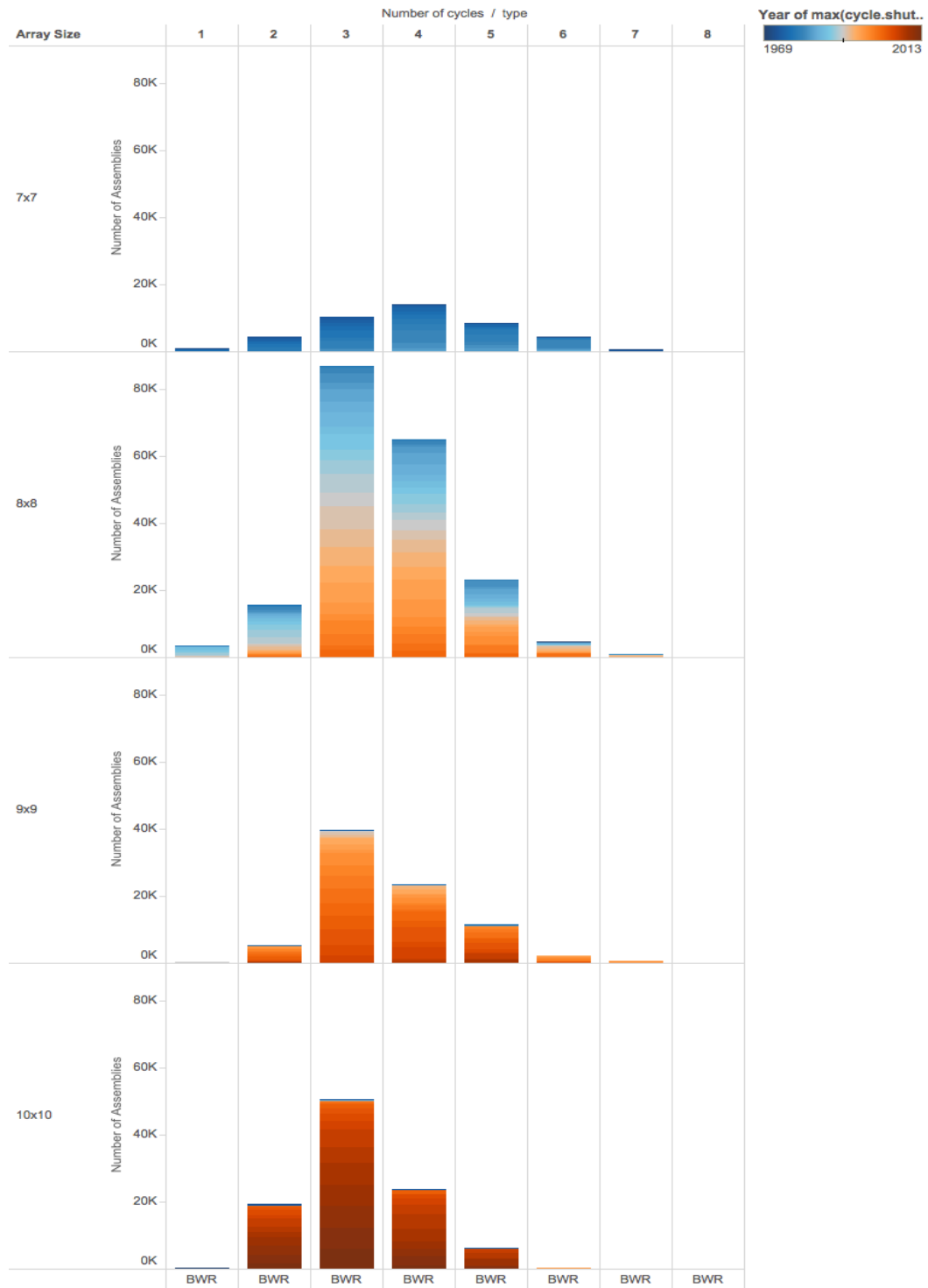
Figure 3.5. Number of irradiation cycles for BWR assemblies in the GC-859 database [17].

3.3   Results

3.3.1   Fuel Temperature

The variation of the cask k_{eff} as a function of the fuel temperature used in the assembly depletion simulation is presented in Figure 3.6 for the AO isotope set and in Figure 3.7 for the AFP isotope set. The data in each figure are fitted with a linear least-squares fit line, which is plotted in green. Both AO and AFP results show trends that are well described by linear trend lines. In Figures 3.6 and 3.7, error bars have been omitted because the bars were smaller than the data markers themselves at ±0.0001 (10 pcm, 1 pcm = 10^{-5}). The legends in Figures 3.6 and 3.7 include the expression of the linear fit (with y as cask k_{eff} and x as temperature in K). The R^2 parameter is also included in the legend. This parameter is a measure of the goodness of fit and varies between 0 and 1, with a value close to 1 indicating a good fit.
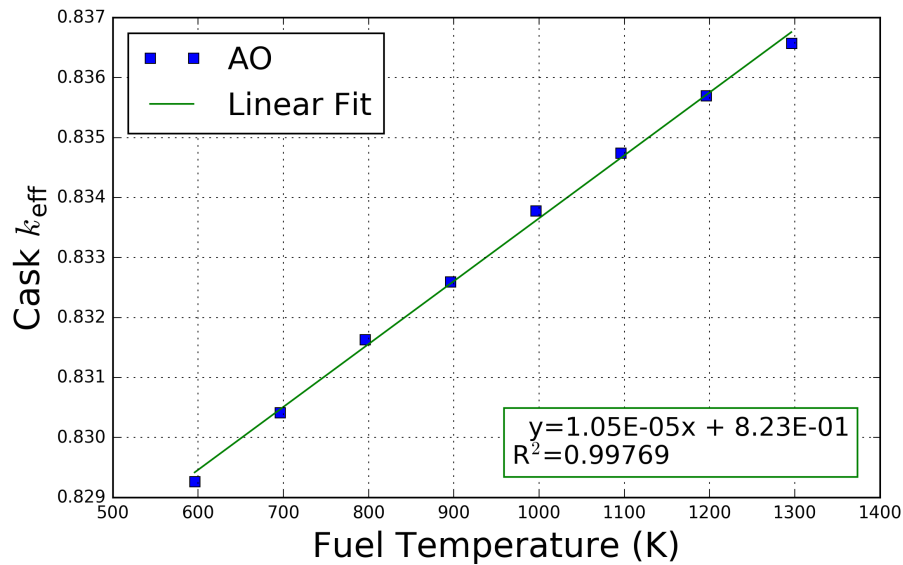
Figure 3.6.   Effect of fuel temperature on cask k_{eff} (AO isotope set).
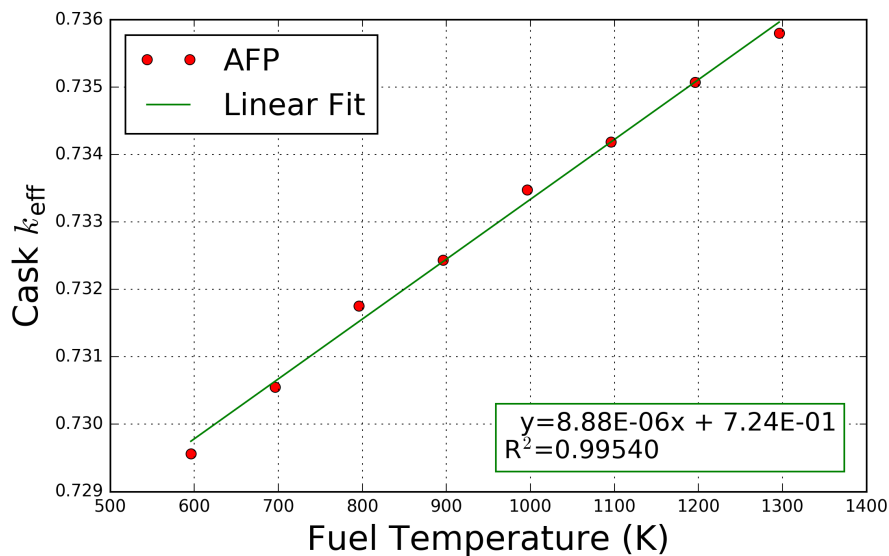
Figure 3.7. Effect of fuel temperature on cask k_{eff} (AFP isotope set).

20

The calculated k_{eff} data illustrated in Figures 3.6 and 3.7 are listed in Table 3.3. This table also includes the k_{eff} differences in pcm relative to the nominal case.

Table 3.3.   Cask reactivity as a function of fuel temperature

Temp. (K)	AO k_{eff}	$1\sigma^a$	AFP k_{eff}	1σ	AO Δk_{eff}^b (pcm^c)	1σ (pcm)	AFP Δk_{eff} (pcm)	1σ (pcm)
596	0.82927	0.00010	0.72957	0.00010	-236	14	-219	14
696	0.83042	0.00010	0.73055	0.00010	-121	14	-121	14
796	0.83163	0.00010	0.73176	0.00010	0		0	
896	0.83259	0.00010	0.73244	0.00010	96	14	68	14
996	0.83378	0.00010	0.73348	0.00010	215	14	172	14
1,096	0.83474	0.00010	0.73419	0.00010	311	14	243	14
1,196	0.83570	0.00010	0.73507	0.00010	407	14	332	14
1,296	0.83658	0.00010	0.73580	0.00010	495	14	404	14

[a] Standard deviation in k_{eff} as reported in the KENO output file
[b] k_{eff} difference relative to the 796K nominal case
[c] 1pcm = 0.00001

The effect of fuel temperature on cask reactivity is clearly linear over the temperature range studied: reactivity increases with increasing temperature, which is consistent with findings from previous studies [5, 14]. The k_{eff} results listed in Table 3.3 are consistent with the expected physics behavior (e.g., resonance Doppler broadening increases with increasing temperature) and are driven by the change in isotopic composition of SNF as a function of temperature during depletion. As expected, the increase in cask k_{eff} with increasing fuel temperature is mainly due to actinides (major contributors ^{235}U, ^{239}Pu, ^{241}Pu), as indicated by the small difference between Δk_{eff} calculated with the AO and AFP isotope sets for the same temperature. The magnitude of the cask reactivity increase is ~1.0 pcm/K for the AO set and ~0.9 pcm/K for the AFP set, based on the linear fits given in Figures 3.6 and 3.7.

The variation of the ^{235}U and ^{239}Pu number densities (in atoms/b-cm units) in all fuel rods as a function of the axial node and for temperatures considered in this study is illustrated in Figure 3.8. Figure 3.8 shows the ^{235}U and ^{239}Pu data corresponding to nominal, minimum, and maximum temperatures to facilitate understanding of the physics. Compared to the nominal case (796 K), when the temperature increases to 1,296 K, the discharge nodal-average ^{239}Pu atomic density increases approximately 6–10% depending on the node. The large step change in the ^{239}Pu number density near 80 inches is due to the change from full to vanished lattice, which significantly changes the neutron spectrum due to the presence of empty lattice locations (more water moderator) in the vanished lattice. Other smaller variations in Figure 3.8 are due to the variations in the axial burnup profile.
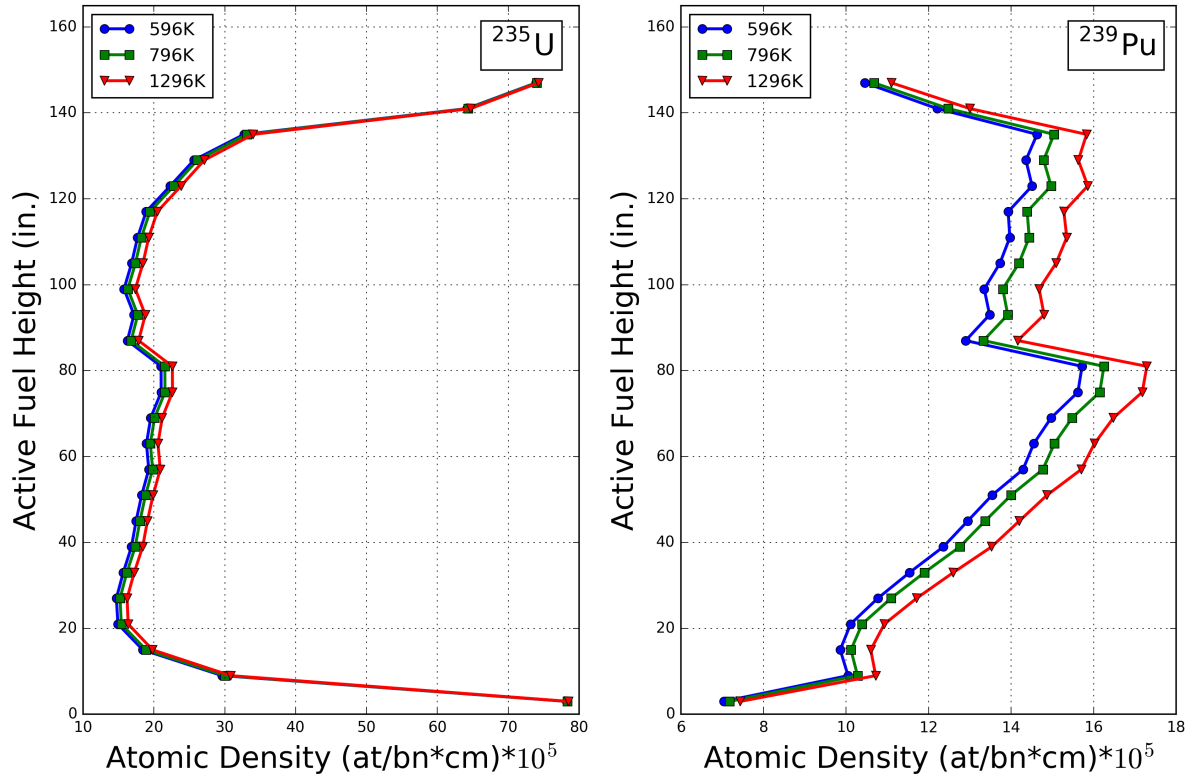
Figure 3.8. Effect of fuel temperature on [235]U and [239]Pu in the non-Gd bearing fuel pins.

3.3.1.1 Fuel Temperature Axial Profile

The effect of the axial temperature distribution on cask reactivity is assessed by comparing fuel temperature profiles with uniform fuel temperatures constructed using the average temperature of the selected axial profiles. As previously stated, all the nodal fuel temperature data were averaged into cycle-average fuel temperature profiles for every fuel assembly, so every profile discussed in this section represented a cycle-averaged profile. The minimum (Min) and maximum (Max) average fuel temperature assemblies were selected and simulated using profiled and uniform axial fuel temperature distributions. These four temperature profiles, along with the cycle- and core-averaged fuel temperature profiles, are plotted in Figure 3.9.

The difference in the calculated cask k_{eff} values comparing the *Min Profile* and *Min Uniform* results are 0.005% and -0.042% Δk_{eff} for the AO and AFP isotope sets, respectively. The difference in the cask k_{eff} results for the *Max Profile* and *Max Uniform* are 0.113% and 0.037% Δk_{eff} for the AO and AFP isotope sets, respectively. As expected, there is a larger impact of using a uniform temperature treatment for the maximum temperature case, as there is a larger variation in the fuel temperature as a function of axial position. The cask k_{eff} values are generally higher when a uniform axial temperature is used because the temperatures in the top nodes of the fuel assembly (of significant importance to cask reactivity) are higher than they are in the cases with nonuniform temperature profiles. This leads to increased plutonium production in the top nodes, slightly increasing cask k_{eff}. Overall, the impact of using uniform versus profiled axial fuel temperatures is very small, on the order of 0.1% Δk_{eff}. Given this level of bias, as well as the direction of the bias, use of uniform axial fuel temperatures is conservative.
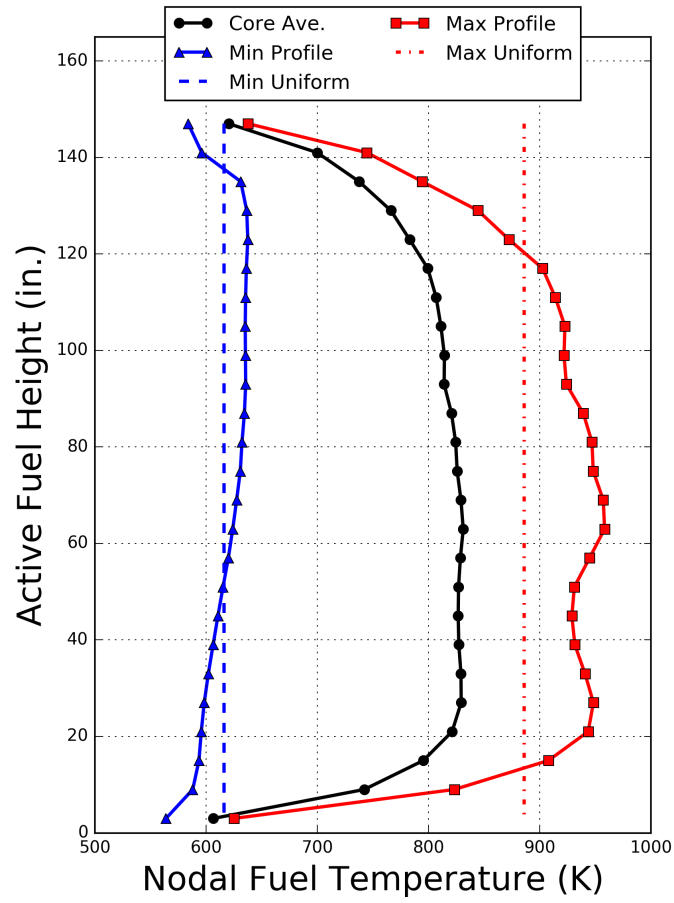
Figure 3. 9. Cycle-average fuel temperature profiles selected to analyze the effect of axial fuel temperature shape on cask reactivity.

3.3.2   Bypass Water Density

The variation of the cask k_{eff} as a function of reduction in the bypass water density during the assembly depletion simulation is presented in Figure 3.10 for the AO isotope set and in Figure 3.11 for the AFP isotope set. For both AO and AFP isotope sets, k_{eff} varies linearly over the considered range of density reduction. The calculated k_{eff} data are presented in Table 3.4.
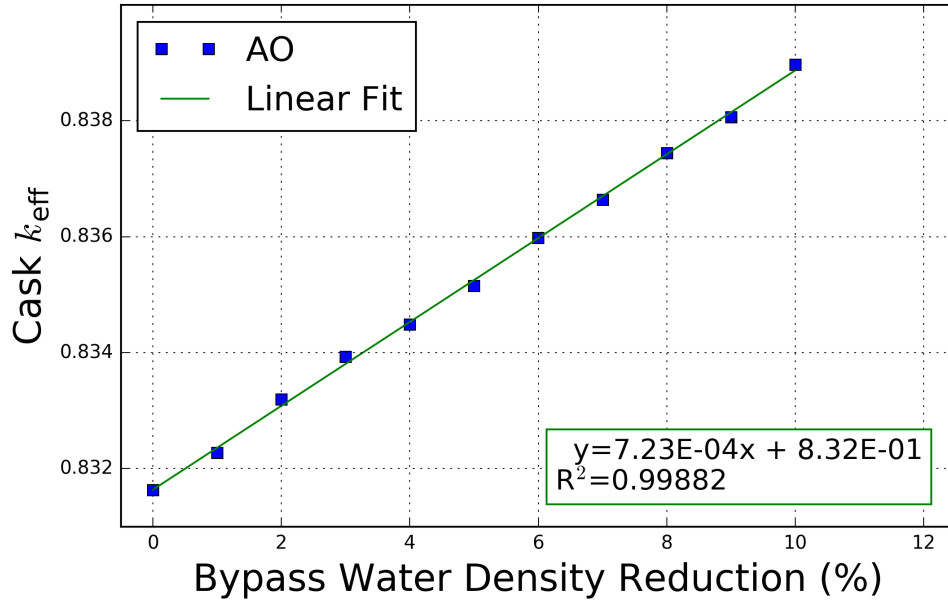
Figure 3.10.   Effect of bypass water density on cask k_{eff} (AO isotope set).
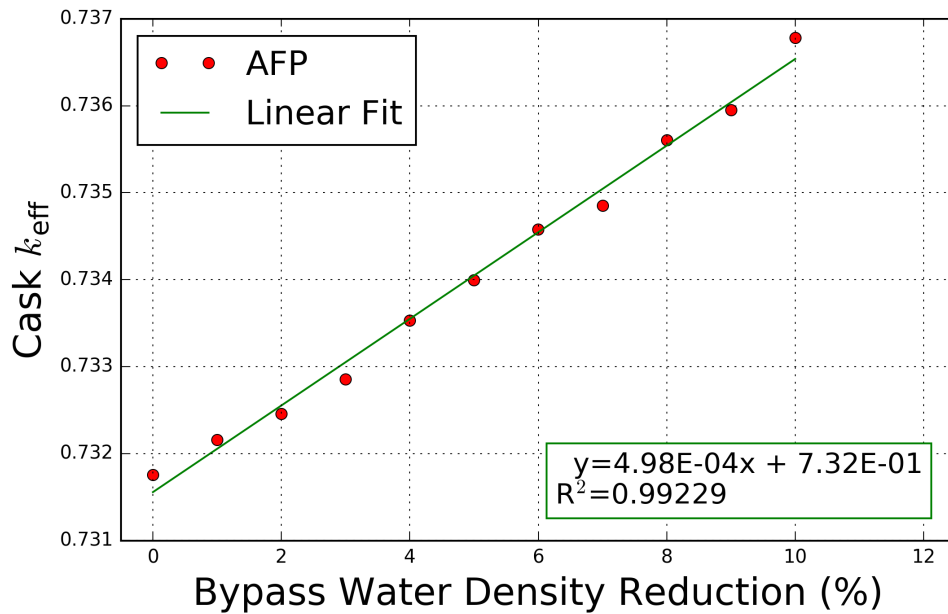
Figure 3.11.   Effect of bypass water density on cask k_{eff} (AFP isotope set).

24

Table 3.4.   Cask reactivity as function of bypass water density reduction

Density reduction (%)	AO k_{eff}	$1\sigma^a$	AFP k_{eff}	1σ	AO Δk_{eff}^b (pcm^c)	1σ (pcm)	AFP Δk_{eff} (pcm)	1σ (pcm)
10	0.83897	0.00010	0.73679	0.00010	735	14	503	13
9	0.83806	0.00010	0.73595	0.00010	643	14	420	14
8	0.83745	0.00010	0.73560	0.00010	582	14	385	14
7	0.83664	0.00010	0.73485	0.00010	501	13	310	14
6	0.83598	0.00010	0.73458	0.00010	435	14	283	14
5	0.83516	0.00010	0.73400	0.00010	353	14	224	14
4	0.83449	0.00010	0.73353	0.00010	286	14	177	14
3	0.83393	0.00010	0.73285	0.00010	230	14	110	14
2	0.83319	0.00010	0.73246	0.00010	156	14	70	14
1	0.83227	0.00010	0.73216	0.00010	64	14	40	14
0	0.83163	0.00010	0.73176	0.00010	0	14	0	14

[a] Standard deviation in k_{eff} as reported in the KENO output file
[b] k_{eff} difference relative to the nominal case (0% density reduction)
[c] 1pcm = 0.00001

A large decrease in the density of the bypass water would lead to a significant hardening of the neutron spectrum based on the amount of water within the large two water rods at the center of the assembly and outside the assembly channel. Consequently, there will be an increase in the production of plutonium isotopes with decreasing bypass water density. The variation of the [235]U and [239]Pu atomic densities in the non-Gd bearing fuel rods as a function of axial position is illustrated in Figure 3.12 for 0%, 5%, and 10% bypass flow density reduction. As seen in Figure 3.12, the impact on [239]Pu content relative to the nominal case is large in both VAN and DOM lattice nodes. In the VAN lattice nodes, the spectrum differs from that in the DOM lattice nodes due to a combination of two effects: hardening due to less moderation (smaller coolant densities), and softening due to fewer fuel rods (larger neutron mean free path); the net effect is a hardening of the spectrum. Water density reduction in the large water rods at the center of the assembly and outside the assembly channel further impacts the neutron moderation in all nodes, with the actual impacts depending on the particular node environment and parameters (coolant density, burnup).

A 10% reduction in the bypass water density relative to its nominal value leads to an increase of the assembly average [239]Pu content of ~7%, and consequently, it also leads to a significant increase in cask reactivity for the studied case. The actual bypass water density is not well known, but it is expected to be bounded by the 10% density reduction value. Even for an unlikely reduction in bypass water density of 10%, the impact on cask reactivity is significantly smaller than the effects of coolant density, axial burnup profile, or control blade usage [4]. Based on the results in this study, irrespective of the isotope set used in criticality calculations, the effect is clearly less than 0.1% Δk_{eff} for every 1% reduction in bypass water density.
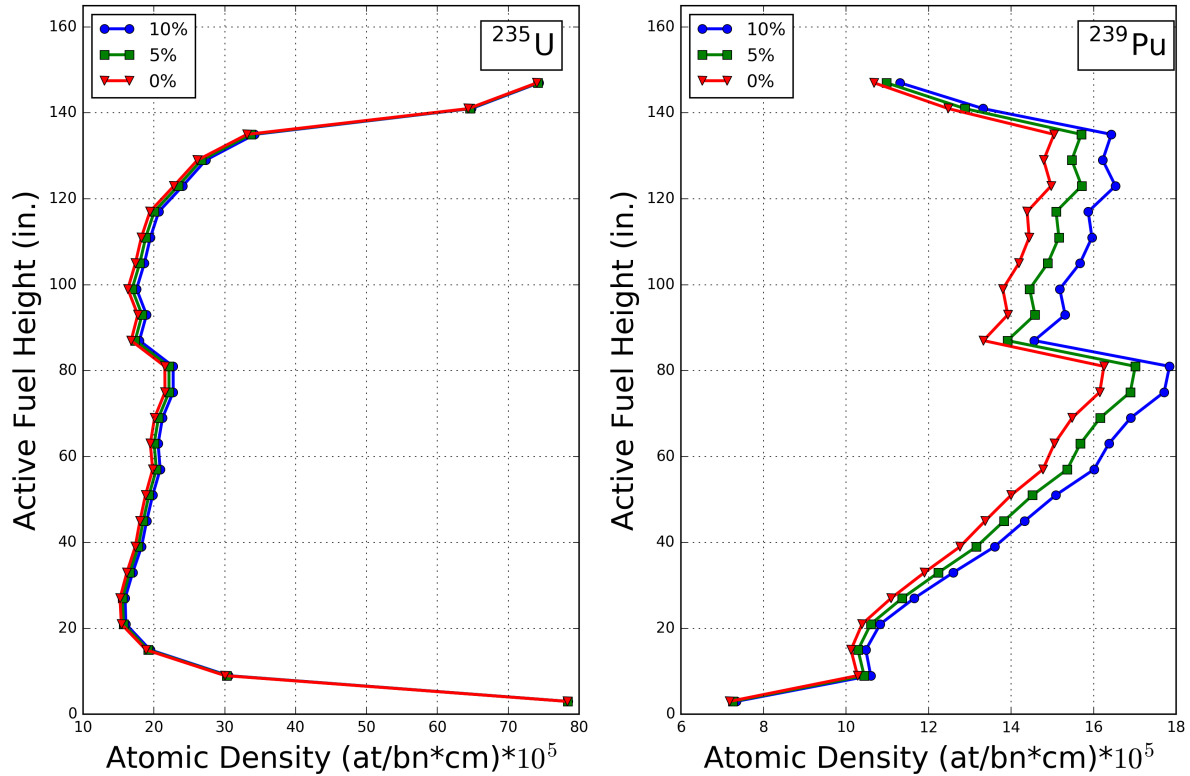
Figure 3.12. Effect of bypass water density on ^{235}U and ^{239}Pu node-averaged atomic density.

3.3.3 Specific Power

As discussed in Sect. 3.2.3, the specific power was changed by ±10% relative to the nominal case, while the irradiation times were adjusted to keep the discharge burnup the same. The impact of these variations on cask reactivity is summarized in Table 3.5 and illustrated in Figure 3.13. Data in Figure 3.13 are plotted with 1σ (statistical uncertainty in k_{eff}) error bars. The effect is extremely small for this magnitude of the specific power variation and not significantly higher than the statistical uncertainty (1σ) in the calculated cask k_{eff}.

The direction and the magnitude of the change in cask reactivity are consistent with the expected behavior and results of previous studies [5,14]. Cask k_{eff} increases with higher specific power for the AO set due to the slight increase in the mass of plutonium isotopes. For example, increasing specific power by 10% results in an increase of less than 0.1% in the content of ^{235}U and less than 0.15% in the content of ^{239}Pu in the considered assembly. Overall, the impacts are on the order of the 2-sigma uncertainty (28 pcm), indicating that there is very little impact on cask reactivity to varying specific power. The ±10% specific power used in this study is meant to test the sensitivity to inaccurately modeling the specific power. The results show that the specific power has a small effect on cask reactivity, although higher specific power may lead to slight increase in cask reactivity. Significant increases in assembly specific power would require corresponding uprates to the core rated power; analysts should take care in correlating the core power with the time the assembly was in the core to generate an accurate estimate for the specific power.

26

Table 3.5. Cask k_{eff} as function of change in specific power

Specific power change	AO		AFP		AO		AFP	
	k_{eff}	$1\sigma^a$	k_{eff}	1σ	Δk_{eff}^b (pcm^c)	1σ (pcm)	Δk_{eff} (pcm)	1σ (pcm)
+10%	0.83196	0.00010	0.73173	0.00010	34	14	-3	14
0%	0.83163	0.00010	0.73176	0.00010	0		0	
-10%	0.83138	0.00010	0.73153	0.00010	-25	14	-22	14

^{a} Standard deviation in k_{eff} as reported in the KENO output file
^{b} k_{eff} difference relative to the nominal case (0% specific power change)
^{c} 1pcm = 0.00001
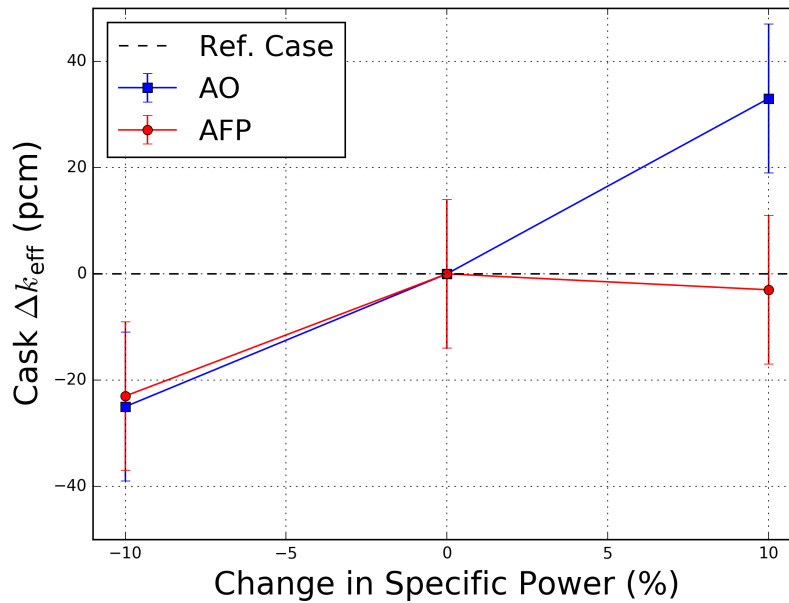
Figure 3.13. Effect of specific power on cask reactivity.

3.3.4 Operating History

The variation of the cask k_{eff} for the operating histories listed in Table 3.1 is presented in Table 3.6. Figure 3.14 shows the impact in k_{eff} for each of the considered histories relative to history OH-1 (which is characterized by 100% power level in each of the three cycles and no downtime between cycles). In general, the trends of these results are similar to those identified in previous studies [14,19].

Table 3.6.   Cask reactivity as function of operating history

Operating History	AO		AFP		AO		AFP	
	k_{eff}	$1\sigma^a$	k_{eff}	1σ	$\Delta k_{eff}^{\ b}$ (pcm^c)	1σ (pcm)	Δk_{eff} (pcm)	1σ (pcm)
OH-1	0.83163	0.00010	0.73176	0.00010	0		0	
OH-2	0.83170	0.00010	0.73154	0.00010	7	14	-21	14
OH-3	0.83099	0.00010	0.73092	0.00010	-63	14	-84	14
OH-4	0.83118	0.00010	0.73144	0.00010	-45	14	-31	14
OH-5	0.83100	0.00010	0.73155	0.00010	-63	13	-21	14
OH-6	0.83126	0.00010	0.73160	0.00010	-37	14	-16	14
OH-7	0.83189	0.00010	0.73170	0.00010	26	14	-6	14
OH-8	0.82987	0.00010	0.73043	0.00010	-175	14	-133	14
OH-9	0.83121	0.00010	0.73110	0.00010	-41	14	-66	14
OH-10	0.83083	0.00010	0.73138	0.00010	-80	14	-38	14

[a] Standard deviation in k_{eff} as reported in the KENO output file
[b] k_{eff} difference relative to operating history OH-1
[c] 1pcm = 0.00001

History OH-1 results in the highest k_{eff}, within statistics. Relative to all other considered histories for either the AO or the AFP isotope sets, the differences in k_{eff} between OH-1 and other histories are either negative or statistically negligible (within two standard deviations). The only cases where the difference is not negative (though the k_{eff} values are within two standard deviations) occur for histories OH-2 and OH-7 with the AO isotope set.

Results for histories OH-1 and OH-2 are statistically equivalent, confirming that neglecting typical downtimes in depletion simulations does not impact cask reactivity, as previously noted [4].

Extended downtime later in an assembly's irradiation history leads to lower cask k_{eff} for both AO and AFP isotope sets. This effect is mainly due to the decay of ^{241}Pu ($T_{1/2}$ = 14.4 yr), an actinide with significant effect on cask reactivity. The magnitude of the reactivity for the AO set is statistically similar (within 2σ) to that for the AFP isotope set. For example, for uniform power operation, an extended downtime before the last irradiation cycle (OH-3 vs. OH-1) leads to a cask k_{eff} decrease of 63 pcm (1σ=14 pcm) for the AO set and 84 pcm (1σ=14 pcm) for the AFP set. These extended downtimes therefore do not require explicit modeling for conservative estimates of cask reactivity.

The effect of extended downtime before the last irradiation cycle shows the same decreasing trend irrespective of the power level history during irradiation. Moreover, the magnitude of the decrease is similar for the AO and AFP sets given the same power history. For example, see the values for OH-3 corresponding to the two isotope sets. Furthermore, the magnitude varies with the cycle down time. Operating histories OH-5 and OH-8 have the same power history (120% for the first two cycles and 60% for the last cycle), but their downtimes are much different before the last cycle (30d vs 720d).
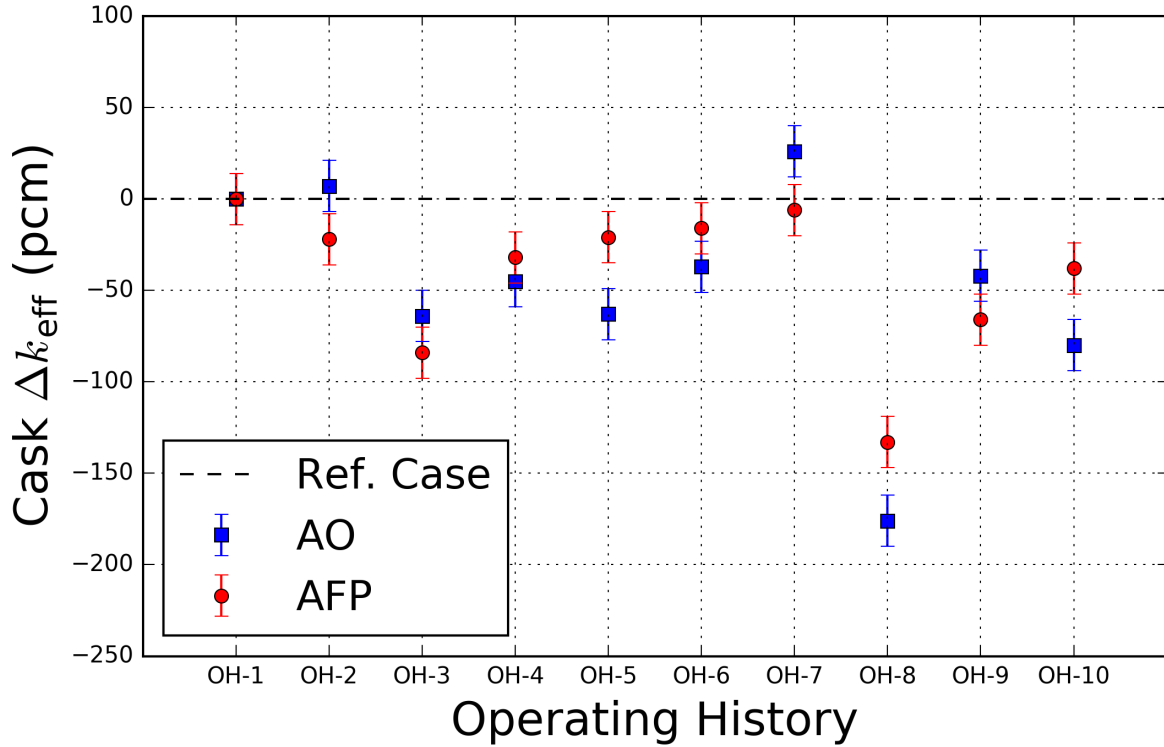
Figure 3.14.   Effect of operating history on cask reactivity.

The decrease in k_{eff} due to extended downtime before the last cycle (OH-8 vs. OH-5) for both the AO and AFP sets is 112 pcm. The magnitude of the decrease is larger in this case than for the uniform power operation (OH-3 vs. OH-1) because more plutonium is produced during the first two cycles (higher burnup at the end of the first two cycles). The effect of the downtime is also observed for operating histories OH-7 and OH-9, both of which have the same power history but different downtimes before the last cycle. Case OH-9 results in a decrease in reactivity of 67 pcm and 60 pcm compared to OH-7 for the AO and AFP isotope sets, respectively. The magnitude of the decrease is slightly less than that observed for uniform power operation (OH-3 vs OH-1), indicating once again that the magnitude of the effect depends on the power history.

Operating histories OH-4 through OH-7 illustrate the effect of the power level variation during irradiation. They all have the same downtime, but they have different, nonuniform power levels. The results indicate that the effect for the AFP isotope set is statistically negligible, within 2σ for all operating histories in this set compared to the reference history OH-1. However, if only the AO isotope set is considered, there is a small but clear effect on the power level in the last two cycles, especially in the last cycle. If the power in the last cycle is higher (OH-7), more plutonium is produced during this cycle, and there is less time for its fissile isotopes to undergo fission before assembly discharge. This results in increased plutonium content in the discharged assembly. For the AO isotope set, the k_{eff} value for OH-7 is 26 pcm higher than for OH-1. However, the two k_{eff} values are within 2σ (1σ = 14 pcm).

The magnitude of the reactivity effects for the AO and AFP sets for history OH-7 are statistically the same (within 2σ). This is likely due to the interplay between the production and decay of those actinides and fission products with high impact on cask reactivity. If the power is higher in the last cycle, then not only does the quantity of actinides increase at discharge, but the quantity of the fission products also increases. This includes ^{155}Eu, which decays with a half-life of 4.75

29

years to ^{155}Gd, a very strong neutron absorber. Therefore, there is an increase in ^{155}Gd present in SNF at 5-year cooling after discharge. In particular, the ^{155}Gd assembly average atomic density for history OH-7 at 5-year cooling is ~2% higher than the corresponding value for history OH-4.

Operating histories OH-8 and OH-9 are intended to illustrate the combined effect of the power level in the last cycle and the downtime preceding the last cycle. The combination of lower power levels during the last cycle and larger downtime preceding this cycle leads to the lowest cask k_{eff} values, as observed in other studies [14].

Operating history OH-10 shows a decrease in reactivity relative to OH-1 for both isotope sets. For the AO set, the reactivity decrease is 80 pcm. For the AFP set, the decrease is smaller, at 38 pcm.

The results obtained for the ten operating histories considered indicate that the use of uniform power levels and no downtime between cycles is a suitable assumption. Case OH-7, has the highest power level in the last cycle and typical downtime, and results in the highest cask reactivity, however, it provides results that are statistically the same as the uniform power and no downtime history.

3.4 <u>Summary and Recommendations</u>

The assessments documented in this section are not fully comprehensive, as they are based on specific assembly and cask configurations, as well as a limited amount of available operating data. The calculated cask reactivity effects are determined for a single assembly average burnup (45.2 GWd/MTHM), but the variations illustrated here are expected to be similar for similar burnup values. Further analysis would be needed to apply these results to significantly different assembly-average burnup values. The established trends in cask reactivity with independent variations of the considered operating parameters are consistent with findings from other studies [5,14,19].

The directions and magnitudes of the impacts on cask reactivity are briefly summarized here for each reactor operating parameter assessed in this section.

Fuel temperature

- Cask reactivity increases linearly with increasing fuel temperature, over the range of 596–1296 K for each of the AO and AFP isotope sets.
- The magnitude of the cask reactivity increase is slightly larger for the AO set than for the AFP set at ~1.0 pcm/K for AO and ~0.9 pcm/K for AFP based on a linear fit in Figures 3.6 and 3.7.
- A bounding value in cask reactivity increase, irrespective of the isotope set used, is 0.12% for every 100 K temperature increase based on data in Table 3.3.
- Use of the highest nodal-average fuel temperature in assembly depletion simulations will lead to the conservative cask reactivity results.

Bypass water density

- Cask reactivity increases with decreasing bypass water density for each of the AO and AFP isotope sets.
- The magnitude of the cask reactivity increase is larger for the AO set than for the AFP set.
- The cask reactivity increase, irrespective of the isotope set used in criticality calculations, is less than 0.1% for every 1% reduction in bypass water density.

Specific power

- Cask reactivity increases with increasing specific power for the AO isotope set, but the magnitude of the increase is very small: ~0.03% for 10% specific power increase based on the data in Table 3.5.
- The cask reactivity effect for the AFP isotope set is negligible based on the data in Table 3.5.
- BWR BUC analyses crediting only the AO isotope set that model a high, bounding specific power during depletion result in highest cask reactivity. For analyses using the AFP isotope set, a reasonable specific power consistent with the expected depletion conditions produces statistically equivalent cask reactivity to higher specific powers.

Operating history

- Typical downtimes of ~30 days between cycles have a negligible impact on cask reactivity.
- Extended downtimes preceding an assembly's last irradiation cycle before being discharged leads to a decrease in cask k_{eff} values. The magnitude of the decrease is similar for the AO and AFP sets.
- Cask reactivity is negligibly affected by the power level during the assembly's last irradiation cycle relative to the lifetime-average power. Cask k_{eff} slightly increases (within 2σ) with increasing power level during the last cycle for the AO set and is practically unchanged for the AFP set (see Figure 3.14).
- Operating history with uniform power levels and no downtime between cycles provides cask reactivity is statistically equivalent or higher than all other tested scenarios.

As expected, the results summarized here confirm that the impacts of the operating parameters under consideration are small relative to the impacts of control blade usage, axial coolant density, and axial burnup profile [4].

4 IMPACT OF ASSEMBLY-SPECIFIC CONDITIONS ON CASK REACTIVITY

4.1 Background

Axial burnup profile, axial coolant density profile, and control blade usage, the three research objectives previously categorized as high priorities [5], were studied separately in NUREG/CR-7224 [4]. Each parameter was individually varied while keeping all the others unchanged. In the present study, the effect of the correlation of these parameters was investigated, as documented in this section. "Assembly-specific conditions", also called "correlated parameters", are a set of conditions that are realistically experienced by an individual fuel assembly. For example, when the control blade is inserted, the assembly power, coolant density, and many other parameters all change accordingly. Modeling the assembly-specific conditions ensures that the operating parameters of interest are correlated. Previous studies [4] used uncorrelated data from different fuel assemblies that result in limiting cask reactivity estimates. The current work studies assembly-specific conditions to (1) confirm that using uncorrelated but limiting values for all operating conditions leads to conservative cask reactivity and (2) to further understand the impact that modeling assembly-specific conditions has on cask reactivity.

Using limiting values for the axial coolant density profile, burnup profile, control blade history, and other parameters will provide a conservative estimate of reactivity. However, simultaneous application of these limiting assumptions may be overly limiting. In reactor operation, it is unlikely that a fuel assembly would simultaneously experience a limiting control blade history (deeply inserted for long periods of time) and a limiting coolant density profile (low moderation due to high power and increased boiling). The impacts of using true operating data correlated between the various conditions are assessed in this section.

To study the effect of the correlation of these parameters, some of the previously used basic assumptions are applied. The operating data employed in this study, the same as in NUREG/CR-7224 [4], are taken from a single cycle of simulated core-follow data from which nodal-averaged conditions are extracted. The conditions extracted for this study are the control blade history, power history (and resulting burnup profile), nodal coolant density, and nodal fuel temperature. The first three conditions were selected because they have been identified as having the highest level of impact on fuel cask reactivity [4,5]. Fuel temperature was also included to identify potential impacts of using the assembly-specific axial fuel temperature profile.

The main goals of this study are to confirm the hypothesis that using individually limiting conditions selected from different fuel assemblies result in conservative cask reactivity estimates, and to understand the range of possible cask reactivity estimates if assembly-specific conditions are used.

4.2 Methodology

4.2.1 Base Conditions

The study of the effect of assembly-specific conditions requires that base conditions for all parameters of interest first be established. The base conditions for the coolant density profile and axial burnup profile were chosen to be the limiting conditions identified in NUREG/CR-7224 [4]. The limiting base burnup profile is challenging to define because it is a function of the assembly burnup and the isotope set used (AO or AFP).

The base burnup profile was chosen based on the results presented in NUREG/CR-7224 [4]. The discharged assembly burnups cover a burnup range from 25 to 50 GWd/MTHM; therefore, a profile that is limiting or near limiting over this entire range is desired. For conservatism, the models used in this study do not include natural uranium or low-enriched blankets. Tables 6.2 and 6.3 in NUREG/CR-7224 [4] present the top 10 most reactive profiles for a range of burnups for both the AO and AFP isotope sets. A review of these tables indicates that Profile 40 is limiting or near limiting for both isotope sets at all three burnups considered. For this reason, Profile 40 was selected as the base profile for the current study.

The base control blade history uses fully withdrawn control blades during the entire irradiation history because fully inserted control blades for the entire irradiation period is overly limiting compared to realistic control blade histories [4]. The base fuel temperature profile is the highest time-averaged and spatially averaged temperature profile from the operating data. The base temperature profile is selected by averaging the temperature over the entire cycle for each node, resulting in a cycle-average profile. Then the cycle-average profiles are averaged axially, resulting in a single temperature value for each fuel assembly. The cycle-average profile with the highest axially averaged temperature is selected.

Figure 4.1 plots the base conditions used in this study. The base burnup profile shown in Figure 4.1 is different than that used in previous studies [4], but the coolant density (void fraction) profile is the same as that used in Section 3 of this report and in NUREG/CR-7224 [4]. Each axial profile shown in Figure 4.1 is taken from a different fuel assembly, which is unrealistic, but it results in conservative estimates of cask reactivity.
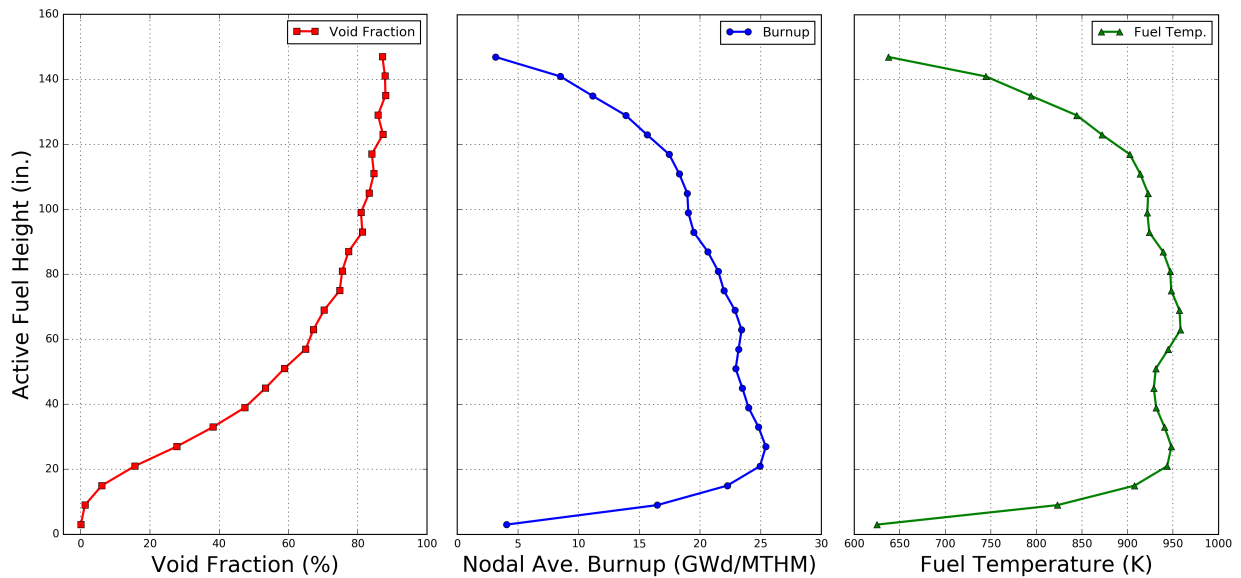
Figure 4.1.   Base conditions used for the coolant void fraction, burnup, and fuel temperature axial profiles.

4.2.2   Assembly-Specific Conditions

The assembly-specific conditions are obtained from the core-follow operating data. To study the impact of using assembly-specific conditions, a simulation is first performed using only the base conditions for all considered parameters. All subsequent calculations use this baseline case as a reference to assess the impact of including the assembly-specific parameters of interest. To test the impact of including as-irradiated conditions, assembly-specific conditions are substituted for base conditions and the cask k_{eff} results are compared to the base conditions. For example,

to assess the impact of assembly-specific control blade insertion, the base condition of control blades removed for the entire irradiation, is replaced with an actual control blade history from a specific assembly. When the assembly-specific conditions are applied, the axial shape and time-dependence of these conditions are both simulated.

Three fuel assemblies were chosen for analysis based on their control blade history and are discussed in this section. Assembly 1 (A1) was chosen because it had the most limiting realistic control blade history, as detailed in in NUREG/CR-7224 [4]. A1 contains two control blade insertions that were near full depth for a significant period of irradiation time. Assembly 2 (A2) was chosen because it had the most cumulative irradiation time where the control blade was inserted (highest control blade history). Detailed control blade histories for A1 and A2 are provided in the results section. Assembly 3 (A3) was chosen as a control; A3 contains no control blade insertion, but it has one of the most limiting burnup profiles identified in NUREG/CR-7224 [4]. A3 will indicate whether the level of conservatism in the base conditions is due primarily to the burnup profile or the other operating conditions.

The cycle-averaged coolant void fraction profiles, axial burnup profiles, and fuel temperature profiles for the base condition and assembly-specific conditions for A1, A2, and A3 are plotted in Figure 4.2. The burnup profiles in Figure 4.2 have been normalized to an assembly-averaged burnup of 25 GWd/MTHM. The burnup profile plot in Figure 4.2 (middle) shows that although the base and A3 burnup profiles were taken from different fuel assemblies, they are very similar. The burnup profiles for A1 and A2 have much higher burnups at the tops of the fuel assemblies than that of A3, which should result in lower cask reactivity for those two assemblies. The coolant void fraction profile plot in Figure 4.2 (left) shows that the base void profile has a higher exit void fraction (lower coolant density) than the three assembly-specific profiles, so the A1–A3 void profiles should result in lower cask reactivity compared to the base profile.
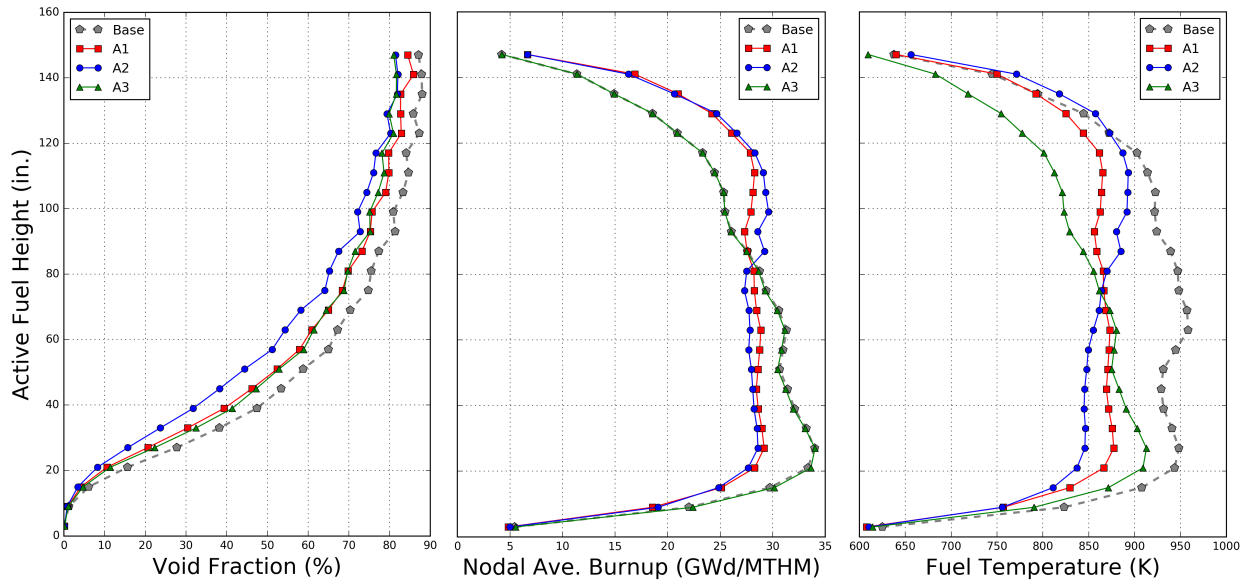
Figure 4.2.   Base and assembly-specific cycle-average conditions for the coolant void fraction, burnup, and fuel temperature axial profiles.

Five calculations are used for each selected assembly to assess the effects of the assembly-specific conditions. Table 4.1 presents a summary of the sequence of these five consecutive calculations. In Table 4.1, the term *base* indicates that base conditions are used (as defined in Figure 4.1), while the term *assembly* indicates that assembly-specific conditions are used for that operating parameter. The first assembly-specific parameter applied is the control blade

insertion. In subsequent calculations, additional conditions are changed one by one, compared to the base case, to ascertain the effect of correlating the operating conditions with control blade insertion.

As identified in Table 4.1, case ID "C" uses the assembly-specific control blade history and base conditions for the coolant density, burnup profile, and fuel temperature. Case ID "CV" uses assembly-specific conditions for the control blade history and coolant density (void fraction), while base conditions are used for the burnup profile and fuel temperature. Likewise, case ID "CVB" uses assembly-specific conditions for the control blade history, coolant density, and burnup profile, while the base fuel temperature is used. Finally, case ID "CVBT" uses assembly-specific conditions for all parameters being tested. The assembly-specific conditions are added one-by-one to enable estimation of the individual effects of each condition, rather than the total of all conditions.

Table 4.1.   Summary of conditions used for correlated parameter calculations

	Operating Parameter			
Case ID	Control Blade	Coolant Density	Burnup Profile	Fuel Temperature
Base	Base (out)	Base	Base	Base
C	Assembly	Base	Base	Base
CV	Assembly	Assembly	Base	Base
CVB	Assembly	Assembly	Assembly	Base
CVBT	Assembly	Assembly	Assembly	Assembly

To model the control blade position as a function of irradiation time for a certain assembly, the irradiation time is divided into intervals that correspond to constant control blade position. Figures 4.3 and 4.4 plot the control blade position as a function of time for assemblies A1 and A2, respectively. In Figure 4.3, the cycle has been divided into five time intervals in which the control blade is either fully withdrawn or inserted to some position as indicated by the gray and white shading and circled numbers labeling each of the five different intervals.

In the calculations that use assembly-specific conditions, both the axial- and time-dependence of the conditions are modeled. The actual operating data contain information on a finer timescale than the changes in control blade elevation. In the correlated parameter calculations, the conditions of interest (nodal coolant density, nodal power, and nodal fuel temperature) are averaged over each time period for which the control blade position is constant. For example, interval 2 of Figure 4.3 is divided into four different time subintervals, the boundaries for which are defined by the interval over which the control blade position is constant. In each of the four subintervals in time interval 2, time-averaged coolant density, nodal power, and fuel temperature are used for each axial node. In interval 2, the axial shape of the assembly-specific conditions is updated four times. The assembly-specific conditions are averaged over any interval during which the control blade position is constant.
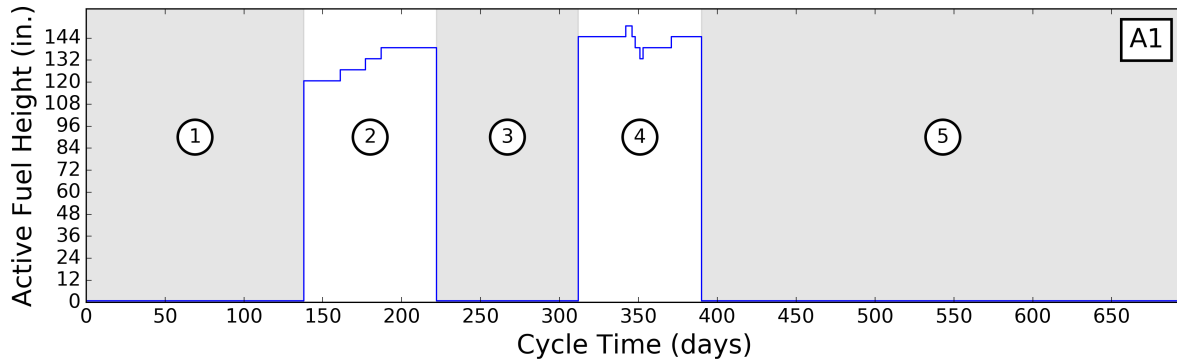
Figure 4.3.   Control blade insertion depth as a function of time for assembly A1.
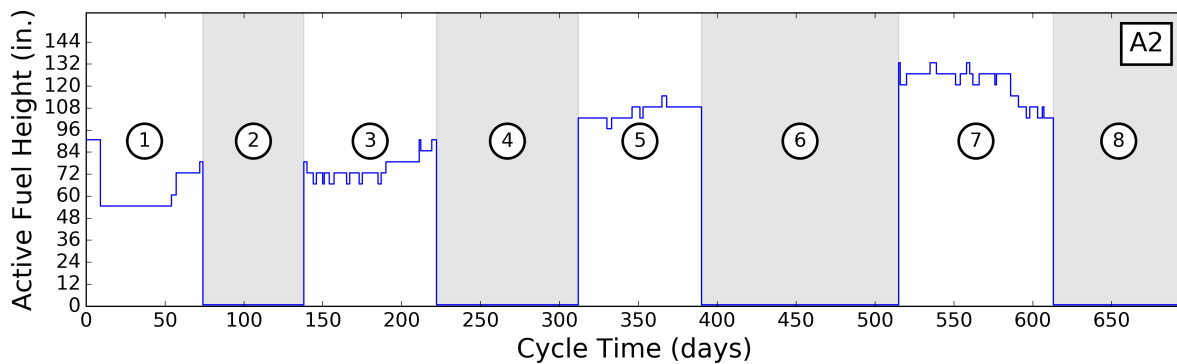
Figure 4.4.   Control blade insertion depth as a function of time for assembly A1.

Two assembly-average discharge burnup values were chosen for analysis: 25 GWd/MTHM and 50 GWd/MTHM. The low burnup value of 25 GWd/MTHM was chosen because it is at the upper limit of a typical single cycle-discharged fuel assembly. The higher burnup value of 50 GWd/MTHM was chosen because it is a value more typical of a discharged fuel assembly. In each of the two discharge burnup cases, the operating data are applied over a single irradiation cycle that spans an irradiation time from BOL until the desired discharge burnup (25 or 50 GWd/MTHM) is reached. This is done by modifying the cycle length while maintaining a certain power level to achieve a burnup of 25 GWd/MTHM and 50 GWd/MTHM. This approach differs from analyses in previous studies, which considered a three-cycle irradiation history. Assessing the impact of assembly-specific conditions over multiple cycles can be performed accurately only where data exist for multiple cycles, which is not the case here. Applying the same control blade history, power, and coolant density history for multiple cycles (as was done in previous calculations for each of the three considered cycles) is likely inadequate for testing the impact of the correlation of the parameters. The results in Section 3 indicate that using no down time between cycles, i.e., one long cycle, has almost no impact on cask reactivity, so this assumption is deemed adequate for this study.

4.3   Results

To fully understand the results and impacts of the control blade insertion on assembly power and other parameters, the fuel assembly irradiation histories for A1 and A2 have been divided into time intervals that correspond to control blades being inserted or fully removed, as labeled

in Figures 4.3 and 4.4. The other parameters of interest have been averaged over these time intervals and plotted in Figure 4.5–4.9 for A1 and Figure 4.10–4.17 for A2.

In Figures 4.3 and 4.4, which depict the control blade insertion depth as a function of time, gray shading used for time interval 1 indicates that the control blades are not inserted; while white shading used for interval 2 indicates that the control blades are inserted. The blue line indicates the axial position of the top of the control blade. These gray or white shaded regions in Figures 4.3 and 4.4 represent the time intervals for which operating data and results are averaged and labeled with identifying numbers. The actual calculations are performed on a finer timescale than the intervals indicated in the figures, as discussed in Section 4.2.2. For A3, plots like those shown for A1 and A2 in Figures 4.3–4.17 have been omitted, as A3 contains no control blade history, so there are no control-blade dependent changes to the plot.

In Figures 4.5–4.9 and 4.10–4.17, three operating condition subplots are included for each of the time intervals. These three subplots are (1) axial coolant void profile (left), (2) specific power for the time interval and total accumulated burnup at the end of that time interval as a function of axial position (middle), and (3) increase in ^{239}Pu concentration during the time interval and the cumulative ^{239}Pu concentration at the end of the time interval as a function of axial position (right). Each operating history plot is labeled in the top left corner with the number of the time interval over which conditions are time-averaged for plotting purposes. The red dashed line in the operating history plots corresponds to the time-averaged control blade tip location for that interval.

As shown in Figures 4.5–4.9, when the control blade is inserted during irradiation, a relatively small impact is observed on the axial void profile. The exit void fraction for step 1 (Figure 4.5) is 86%, and then it drops only to 77% when the blade is inserted in step 2 (Figure 4.6). The exit void fraction then increases to 87% for step 3 (Figure 4.7) when the blade is removed, and then it decreases to 78% in step 4 (Figure 4.8) when the blade is inserted again. This indicates that near full-depth control blade insertion shifts the exit void fraction on the order of 10%, while the impact on the power density is much larger than 10%.

The effect of control blade insertion on the axial power shape is more pronounced than the void profile, as observed in step 2 (Figure 4.6). In step 2, the control blade is inserted to approximately ¾ of full-depth, pushing additional power to the top of the fuel assembly. Then, when the control blade is removed in step 3 (Figure 4.7), the axial power shape becomes significantly bottom-peaked because power has been suppressed for an amount of time in that location. At step 5 (Figure 4.9), most of the fissile material has been consumed at the bottom of the fuel assembly, and power is shifted to the top of the fuel assembly, leading to increased plutonium production in that portion of the fuel assembly.

For A2 (Figures 4.10-4.17), the impact of control blade insertion on the axial power profile and axial burnup profile is much more apparent than for A1. For A2, the control blade is inserted to ~50% full depth, much less than in A1, resulting in significant changes to the axial power shape. In A1, the control blade is inserted to near full-depth, causing a significant change in the magnitude, but little change in the shape of the power density. Similar to A1, insertion of the control blade in A2 has a relatively small impact on the exit void fraction—generally less than 10% when comparing steps with the blade inserted to those with the blade removed.
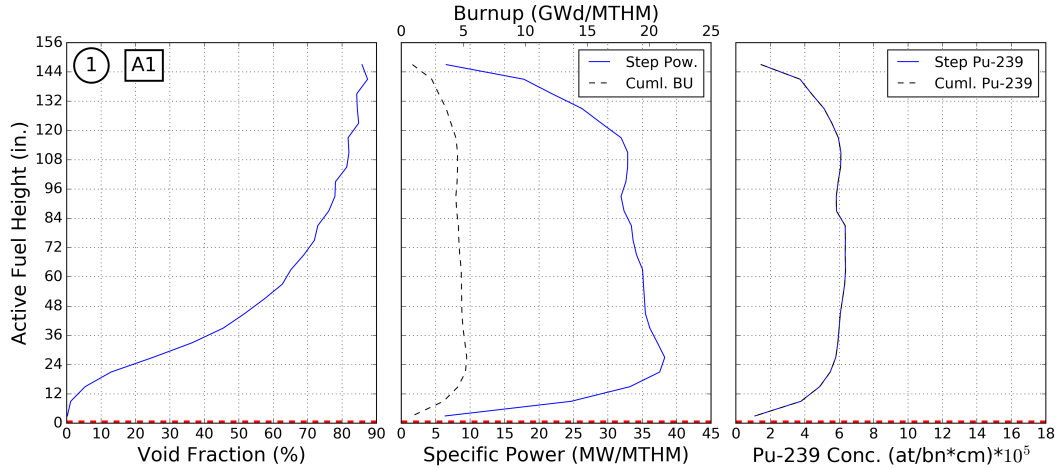
Figure 4.5. Axial coolant void profile, axial-specific power and burnup profile, and axial ^{239}Pu concentration as a function of time for A1 during time interval 1.
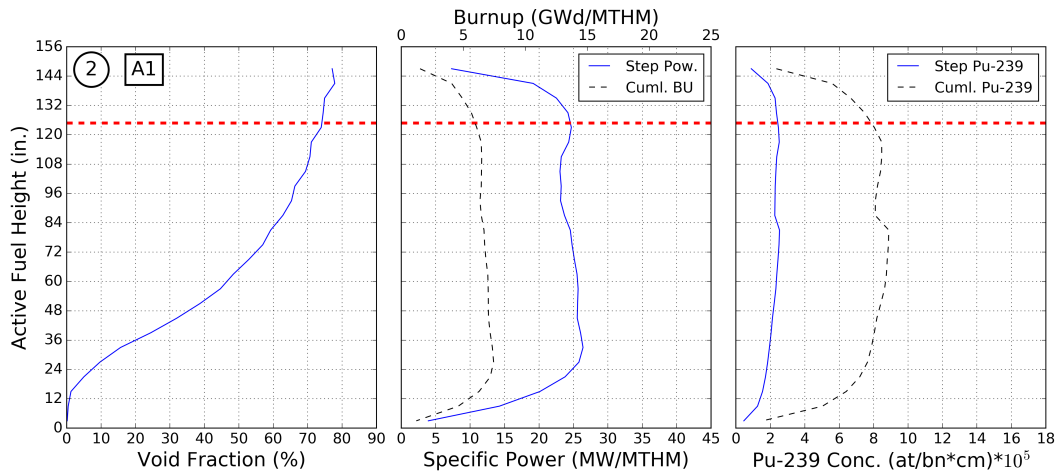
Figure 4.6. Axial coolant void profile, axial-specific power and burnup profile, and axial ^{239}Pu concentration as a function of time for A1 during time interval 2.
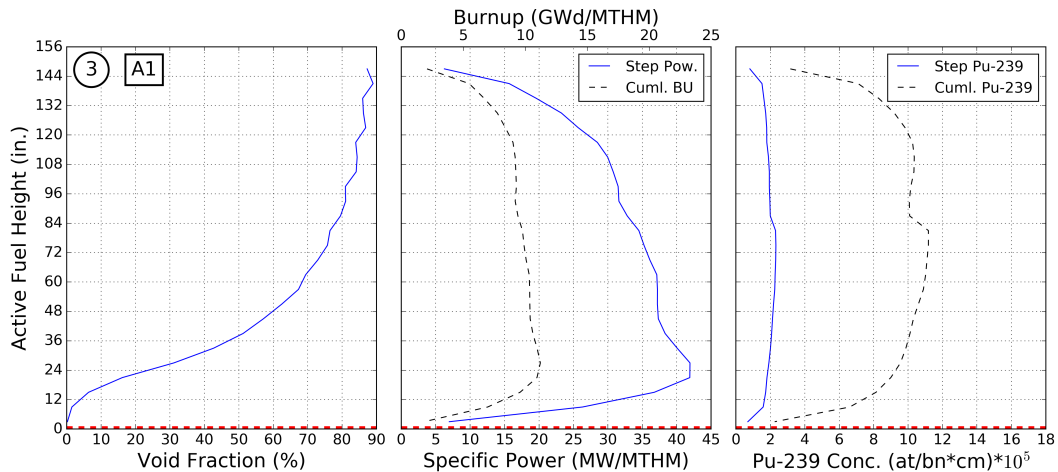
Figure 4.7. Axial coolant void profile, axial-specific power and burnup profile, and axial ^{239}Pu concentration as a function of time for A1 during time interval 3.

Figure 4.8. Axial coolant void profile, axial-specific power and burnup profile, and axial [239]Pu concentration as a function of time for A1 during time interval 4.

Figure 4.9. Axial coolant void profile, axial-specific power and burnup profile, and axial [239]Pu concentration as a function of time for A1 during time interval 5.

Figure 4.10. Axial coolant void profile, axial-specific power and burnup profile, and axial [239]Pu concentration as a function of time for A2 during time interval 1.

40

Figure 4.11.   Axial coolant void profile, axial-specific power and burnup profile, and axial ^{239}Pu concentration as a function of time for A2 during time interval 2.
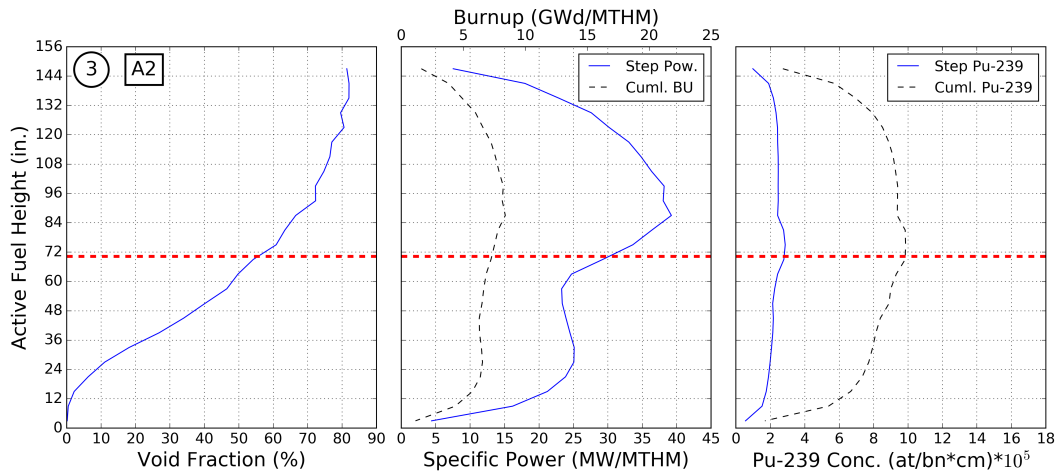
Figure 4.12.   Axial coolant void profile, axial-specific power and burnup profile, and axial ^{239}Pu concentration as a function of time for A2 during time interval 3.
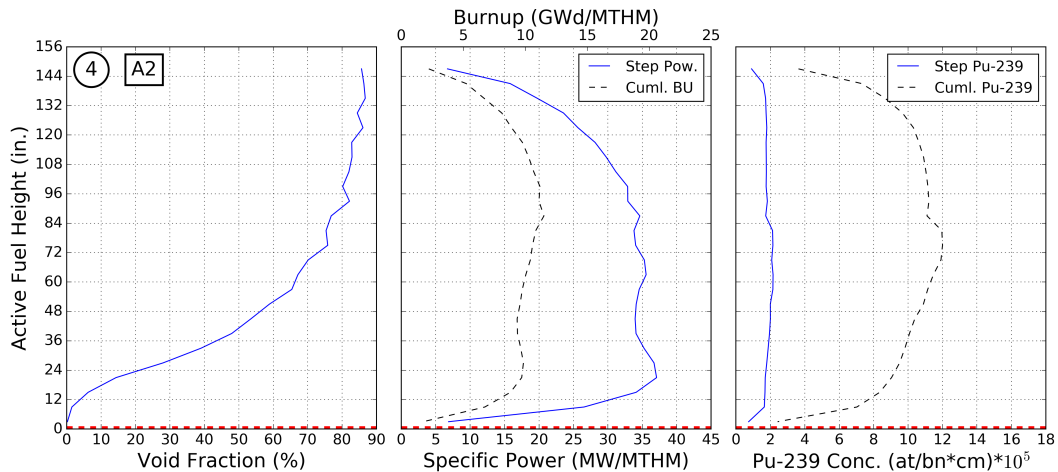
Figure 4.13.   Axial coolant void profile, axial-specific power and burnup profile, and axial ^{239}Pu concentration as a function of time for A2 during time interval 4.
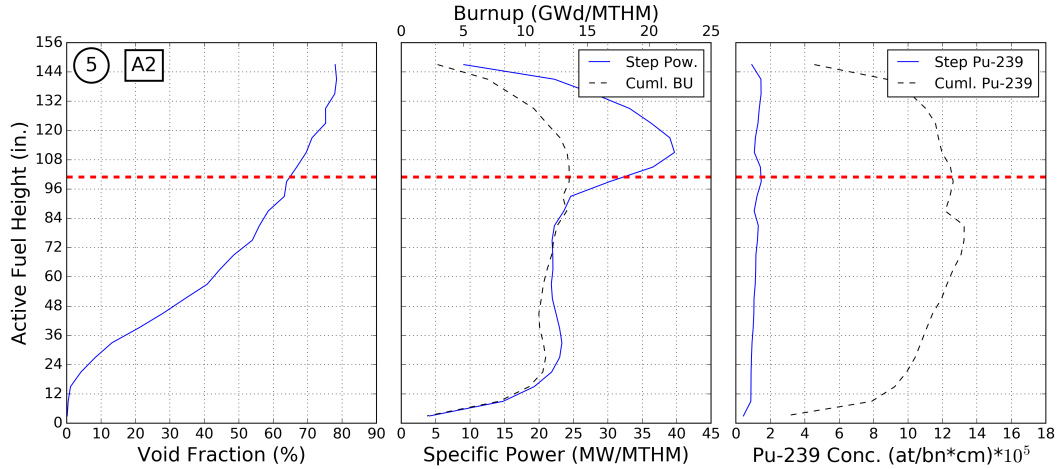
Figure 4.14. Axial coolant void profile, axial-specific power and burnup profile, and axial [239]Pu concentration as a function of time for A2 during time interval 5.

Figure 4.15. Axial coolant void profile, axial-specific power and burnup profile, and axial [239]Pu concentration as a function of time for A2 during time interval 6.
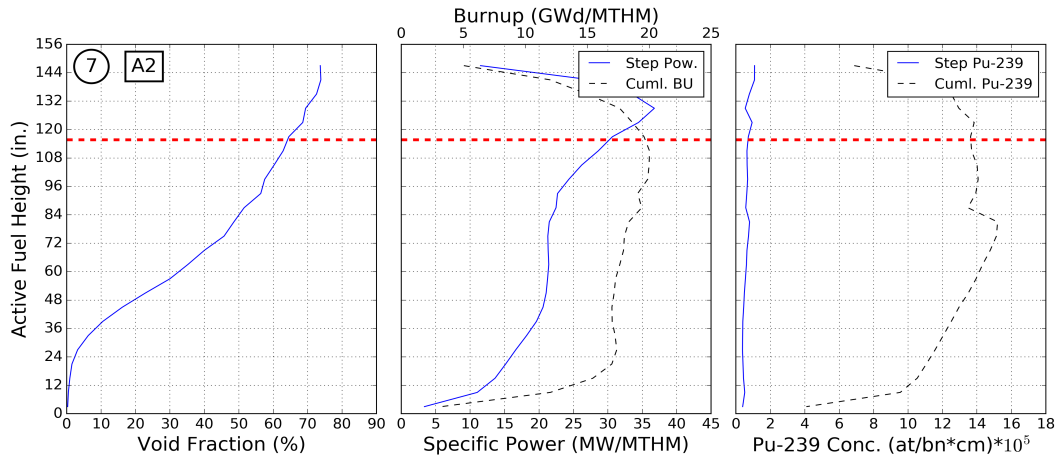
Figure 4.16. Axial coolant void profile, axial-specific power and burnup profile, and axial [239]Pu concentration as a function of time for A2 during time interval 7.
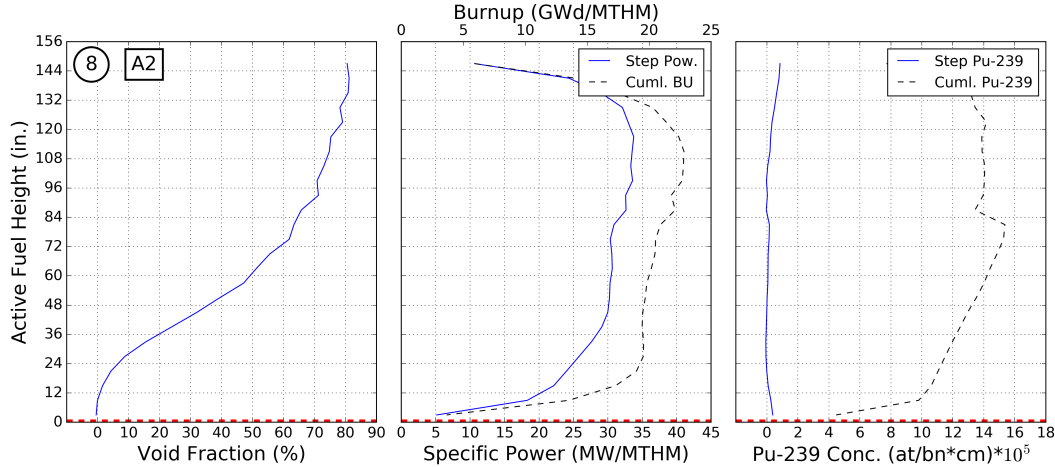
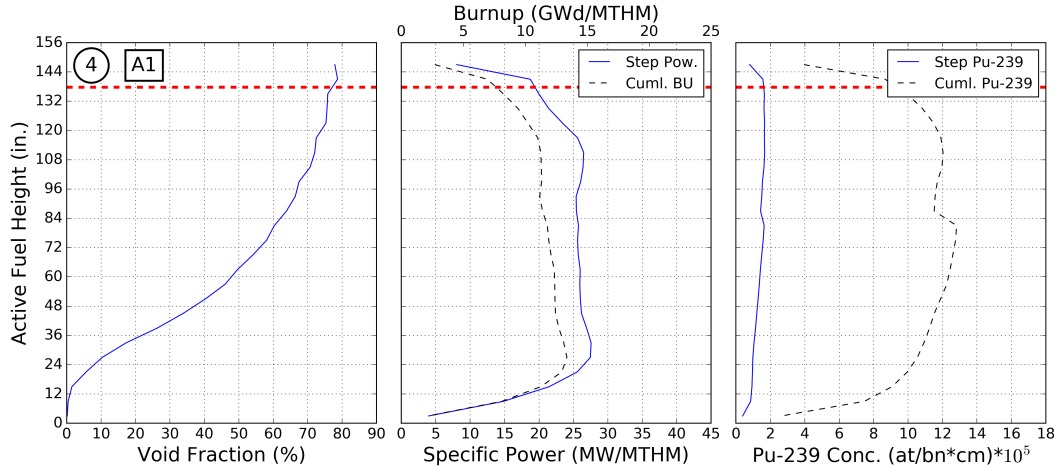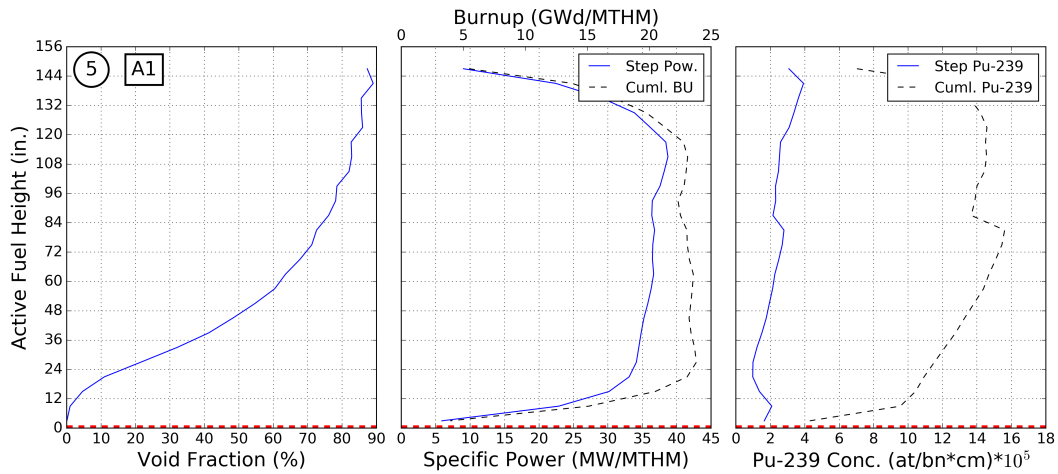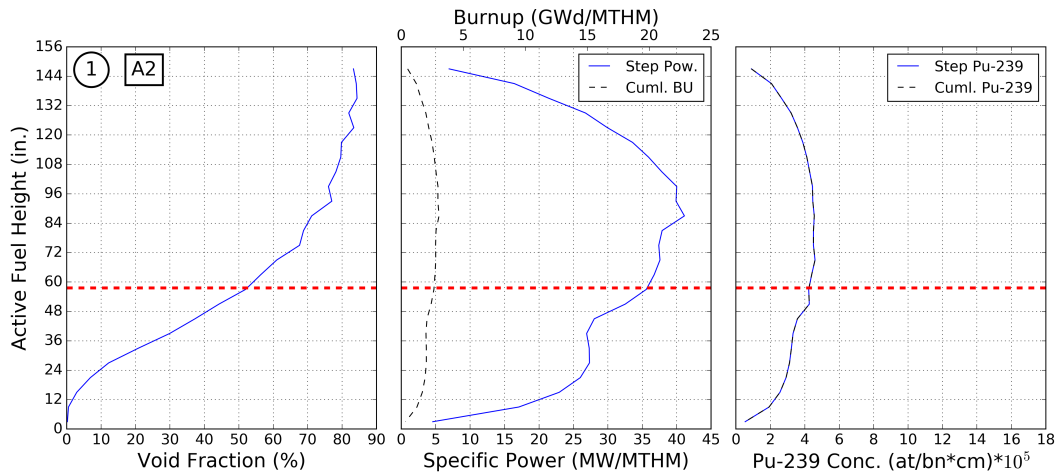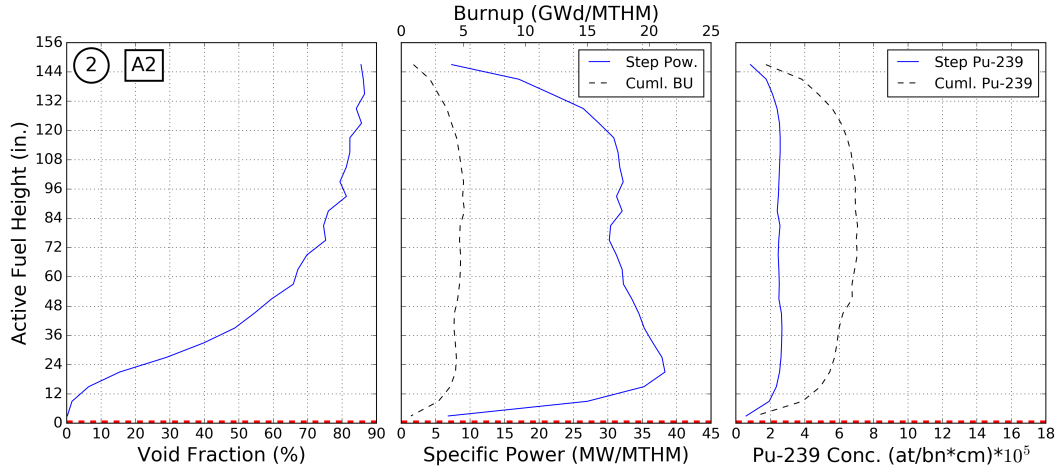**Figure 4.17.** **Axial coolant void profile, axial-specific power and burnup profile, and axial ^{239}Pu concentration as a function of time for A2 during time interval 8.**
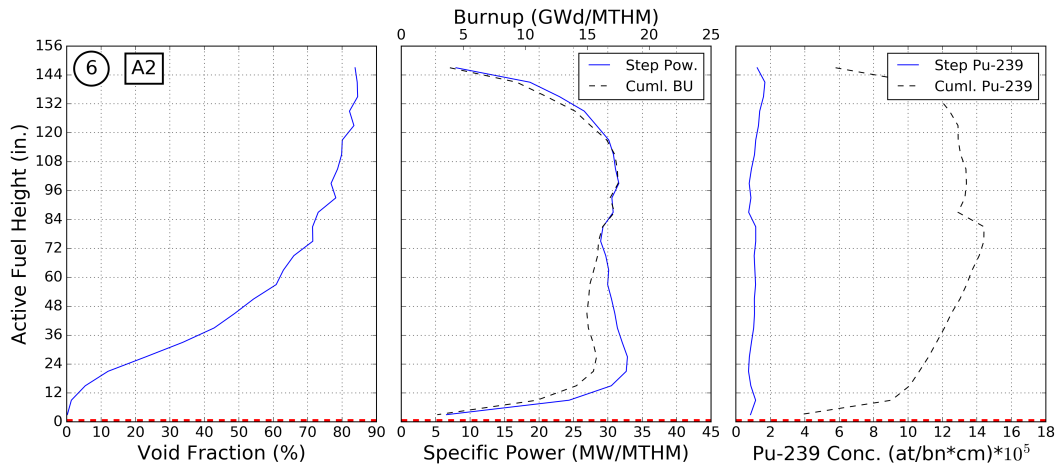
The effect of assembly-specific conditions on cask reactivity is presented in Tables 4.2 and 4.3 for the AO and AFP isotope sets at an assembly average discharge burnup of 25 GWd/MTHM. These tables contain cask k_{eff} values for the five tested cases: base, C, CV, CVB, and CVBT for A1, A2, and A3, as well as differences in cask k_{eff} relative to the base case (Δk_{eff}). The Δk_{eff} values have been plotted in Figure 4.18 for the AO and AFP isotope sets. The dashed lines in this figure indicate the base case reactivity (Δk_{eff} is zero). As discussed in Section 4.2.1, the base cases assumed limiting conditions and control blades completely withdrawn. Any data above this dashed line represent an increase in cask reactivity above the base conditions; likewise, any data below the dashed line represent a decrease in cask reactivity relative to the base conditions.

For A1 and A2, use of the assembly-specific control blade history (C cases) results in a relatively small impact on cask reactivity of less than 1% Δk_{eff} for both the AO and AFP isotope sets. Although these studies are slightly different than those previously documented, this result aligns well with the results in NUREG/CR-7224 [4], indicating an impact of less than 1% on cask reactivity for realistic control blade usage.

The addition of the assembly-specific coolant density profile to the assembly-specific control blade history results in a reduction in reactivity for all cases, although the magnitude of the reduction depends largely on the assembly-specific coolant density profile itself. The reduction in reactivity when comparing C to CV is larger (~500 pcm, or 0.5% Δk_{eff}) for A2 than for the other two assemblies. This is primarily caused by a less limiting coolant density profile (shown in Figure 4.2) for A2 compared to A1 and A3. Overall, using the assembly-specific control blade and coolant density data results in small impacts to cask reactivity.

As shown in Figure 4.18, the largest impact to cask reactivity for the assemblies that contain control blade insertion is clearly the addition of the assembly-specific burnup profile. The magnitude of the impact of the burnup profile varies for each fuel assembly. For the rodded assemblies (A1 and A2), the burnup profile is worth 2–3% Δk_{eff} at 25 GWd/MTHM (comparing CV to CVB). Control blade insertion alone does not have a significant impact on reactivity, but the presence of the control blade during irradiation has a relatively significant impact on the burnup profile. Because control blades in BWRs are inserted from the bottom of the assembly, the power and thus the burnup profile tend to be more top-peaked during periods of control blade insertion. This leads to a reduction in fissile ^{235}U in the upper portion of the fuel assembly,

43

resulting in a large impact compared to one of the limiting burnup profiles. Control blade usage tends to result in less limiting burnup profiles than the cases with no control blade insertion.

For all cases, the impact of including fuel temperature is very small compared to the inclusion of the other three operating conditions. This is expected from the results in Section 3.3.1, which show that the impact of fuel temperature on cask reactivity is on the order of ~1 pcm/K. Section 3.3.1 also shows that the effect of the fuel temperature profile on cask reactivity is small. Overall, the impact of including the fuel temperature in the assembly-specific conditions study is very small compared to the other parameters considered.

The results for A3 are significantly different than the results for A1 and A2. This is largely due to the difference in the operating history for A3 compared to the operating histories for A1 and A2. A1 and A2 were specifically chosen because their operating histories contain significant control blade insertion, leading to changes to other assembly-specific conditions. A3 was chosen because it has no control blade insertion and had one of the more limiting burnup profiles. Because A3 has no control blade insertion, there is little impact to using the assembly-specific conditions for that fuel assembly. However, cask reactivity is slightly lowered by using the assembly-specific conditions for A3, which is primarily due to a less limiting coolant density profile. The magnitude of the reduction in cask reactivity for A3 is much smaller than that obtained for A1 or A2.

Table 4.2. **Cask reactivity data for the AO isotope set at 25 GWd/MTHM**

Case ID	A1 k_{eff}[a]	A2 k_{eff}[a]	A3 k_{eff}[a]	A1 Δk_{eff}[b]	A2 Δk_{eff}[b]	A3 Δk_{eff}[b]
Base	0.89955	0.89955	0.89955	0.00%	0.00%	0.00%
C	0.90316	0.90111	0.89963	0.36%	0.16%	0.01%
CV	0.90122	0.89714	0.89688	0.17%	-0.24%	-0.27%
CVB	0.88050	0.86472	0.89773	-1.91%	-3.48%	-0.18%
CVBT	0.88030	0.86516	0.89720	-1.93%	-3.44%	-0.24%

[a] Standard deviation is 0.00010 for k_{eff} and 0.00014 for Δk_{eff} in all cases
[b] Δk_{eff} relative to base

Table 4.3. **Cask reactivity data for the AFP isotope set at 25 GWd/MTHM**

Case ID	A1 k_{eff}[a]	A2 k_{eff}[a]	A3 k_{eff}[a]	A1 Δk_{eff}[b]	A2 Δk_{eff}[b]	A3 Δk_{eff}[b]
Base	0.81705	0.81705	0.81705	0.00%	0.00%	0.00%
C	0.82116	0.82304	0.81691	0.41%	0.60%	-0.01%
CV	0.81969	0.81793	0.81499	0.26%	0.09%	-0.21%
CVB	0.80992	0.80042	0.81488	-0.71%	-1.66%	-0.22%
CVBT	0.80964	0.79965	0.81415	-0.74%	-1.74%	-0.29%

[a] Standard deviation is 0.00010 for k_{eff} and 0.00014 for Δk_{eff} in all cases
[b] Δk_{eff} relative to base

Figure 4.18. Cask Δk_{eff} values for the AO (left) and AFP (right) isotope sets at an assembly average discharge burnup of 25 GWd/MTHM.

The effect of assembly-specific conditions on cask reactivity can be found in Tables 4.4 and 4.5 for the AO and AFP isotope sets at an assembly average discharge burnup of 50 GWd/MTHM. These two tables contain cask k_{eff} values, as well as the difference in k_{eff} (Δk_{eff}) relative to the base case. Figure 4.19 plots Δk_{eff} values for the four tested cases at an assembly average discharge burnup of 50 GWd/MTHM. The C and CV cases have Δk_{eff} values similar to those of the 25 GWd/MTHM cases, but the impact of the burnup profile is much larger for the 50 GWd/MTHM cases than for the 25 GWd/MTHM cases. The larger impact of the burnup profile compared to the other parameters is due to the more top-peaked fission density axial profiles for the 50 GWd/MTHM cases, as discussed below. Note that in these studies, full-length fuel without natural uranium blankets were modeled; as such, the impact of the burnup profile and other parameters would change depending on the assumptions used model the fuel assembly.

45

Table 4.4.   **Cask reactivity data for the AO isotope set at 50 GWd/MTHM**

Case ID	A1 k_{eff}[a]	A2 k_{eff}[a]	A3 k_{eff}[a]	A1 Δk_{eff}[b]	A2 Δk_{eff}[b]	A3 Δk_{eff}[b]
Base	0.83834	0.83834	0.83834	0.00%	0.00%	0.00%
C	0.84310	0.83919	0.83824	0.48%	0.08%	-0.01%
CV	0.84022	0.83334	0.83389	0.19%	-0.50%	-0.44%
CVB	0.79733	0.77012	0.83364	-4.10%	-6.82%	-0.47%
CVBT	0.79754	0.77073	0.83288	-4.08%	-6.76%	-0.55%

[a] Standard deviation is 0.00010 for k_{eff} and 0.00014 for Δk_{eff} in all cases
[b] Δk_{eff} relative to base

Table 4.5.   **Cask reactivity data for the AFP isotope set at 50 GWd/MTHM**

Case D	A1 k_{eff}[a]	A2 k_{eff}[a]	A3 k_{eff}[a]	A1 Δk_{eff}[b]	A2 Δk_{eff}[b]	A3 Δk_{eff}[b]
Base	0.76000	0.76000	0.76000	0.00%	0.00%	0.00%
C	0.76547	0.76126	0.75999	0.55%	0.13%	0.00%
CV	0.76242	0.75545	0.75569	0.24%	-0.46%	-0.43%
CVB	0.71189	0.68802	0.75531	-4.81%	-7.20%	-0.47%
CVBT	0.71154	0.68877	0.75445	-4.85%	-7.12%	-0.55%

[a] Standard deviation is 0.00010 for k_{eff} and 0.00014 for Δk_{eff} in all cases
[b] Δk_{eff} relative to base

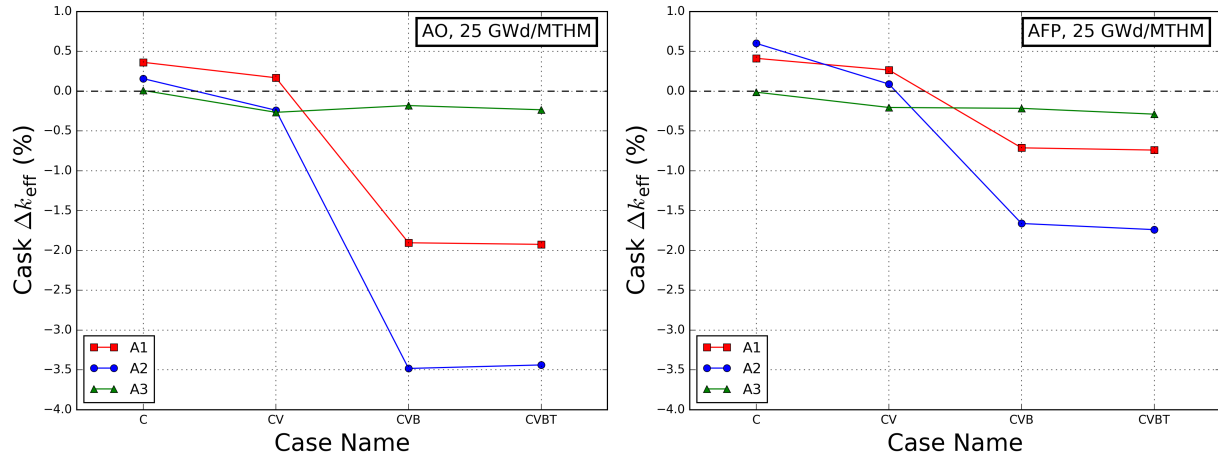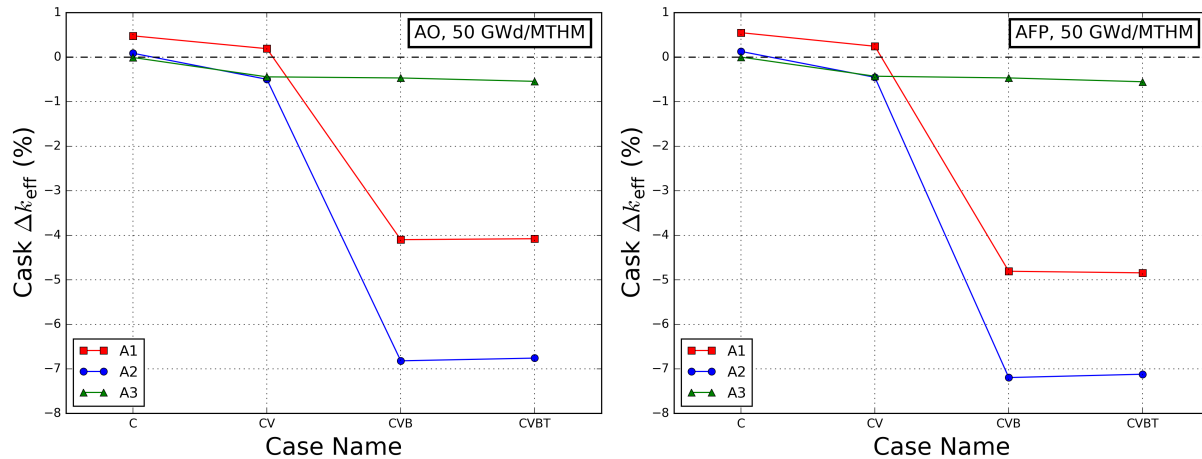**Figure 4.19. Cask Δk_{eff} values for the AO (left) and AFP (right) isotope sets at an assembly average discharge burnup of 50 GWd/MTHM.**

The shape of the curves in Figure 4.19 are similar to those in Figure 4.18, but the impact of the assembly-specific conditions is significantly greater at assembly average burnups of 50 GWd/MTHM than at 25 GWd/MTHM. Specifically, the impact of adding the assembly-specific burnup profile is more significant at 50 than at 25 GWd/MTHM. This is caused by the shape of the axial fission distribution at 25 GWd/MTHM, which is less top-peaked than at 50 GWd/MTHM. Plots of the axial fission distributions for the CVBT cases for the AO and AFP isotope sets at 25 and 50 GWd/MTHM are shown in Figure 4.20. As discussed in this and previous reports, the fission density distribution in the top axial portion of the fuel assembly plays a major role in cask reactivity. The more top-peaked the distribution is, the higher the

impact of the burnup profile on cask reactivity [4]. The cases considered here have a less top-peaked fission distribution at 25 GWd/MTHM compared to that for 50 GWd/MTHM, so the importance of the assembly-specific burnup profile is lessened for the lower burnup.

Figure 4.21 plots the base burnup profile and the assembly-specific burnup profile for A1, as well as the relative burnup difference as a function of axial position. The relative burnup difference for each axial position is calculated as the absolute value of the difference between 1.0 and the ratio of the burnup values at that position for the assembly-specific and base profiles (equation given on the plot). As shown in the figure, the base burnup profile has much lower burnup values at the top of the fuel assembly compared to those in the A1 assembly profile. Correlating that with the more top-peaked fission distribution at 50 GWd/MTHM as shown in Figure 4.20 indicates that the impact of the burnup profile for the higher burnup is primarily due to the large difference in the burnup profiles at the top of the fuel assembly. The relative burnup difference is plotted rather than the absolute difference because high burnup regions in the axial middle of the assembly have a relatively small impact on cask reactivity compared to the low burnup axial top regions. The same absolute burnup difference is worth more in terms of cask reactivity at the top than in the middle of the assembly. Plotting the relative difference in burnup provides a better indication of the impact that burnup difference will have on cask reactivity. Figure 4.21 clearly illustrates that the top portion of the fuel assembly is very important for cask reactivity, and it highlights the importance of the axial fission distribution.

The less top-peaked fission density distribution at 25 GWd/MTHM is a result of the combined impact of the increased residual ^{235}U in the middle axial regions of the fuel assembly, the lower concentration of ^{239}Pu at the top of the assembly, and the higher concentration of residual gadolinium in the top of the fuel assembly. Figure 4.22 shows the ^{235}U, ^{239}Pu, and ^{155}Gd concentration plotted as a function of axial position for assembly A1.

The distribution of the ^{235}U concentration as a function of axial position follows an inverse shape of the burnup profile: it has higher concentrations for lower burnup regions and lower concentrations for higher burnup regions. At both 25 and 50 GWd/MTHM, the ^{235}U concentration is higher at the axial ends of the fuel assembly than in the middle portions of the fuel assembly. Comparing the ^{239}Pu concentration as a function of axial position for the two selected burnups (Figure 4.22, middle) reveals that the 50 GWd/MTHM burnup results in higher plutonium concentrations in the top axial portion of the assembly. For the gadolinium BA, the 25 GWd/MTHM case results in higher ^{155}Gd concentrations in the top and bottom of the assembly due to the lower burnup at the ends of the fuel assembly.

The fission distribution for the AO isotope set (Figure 4.20, left), which does not contain gadolinium, shows that the 50 GWd/MTHM case is more top-peaked than the 25 GWd/MTHM case. However, it is clear that the gadolinium has an impact at 25 GWd/MTHM, as seen by comparing the fission distributions for the AO and AFP isotope sets in Figure 4.20. The AFP fission distribution is clearly less top-peaked than the AO fission distribution at 25 GWd/MTHM.
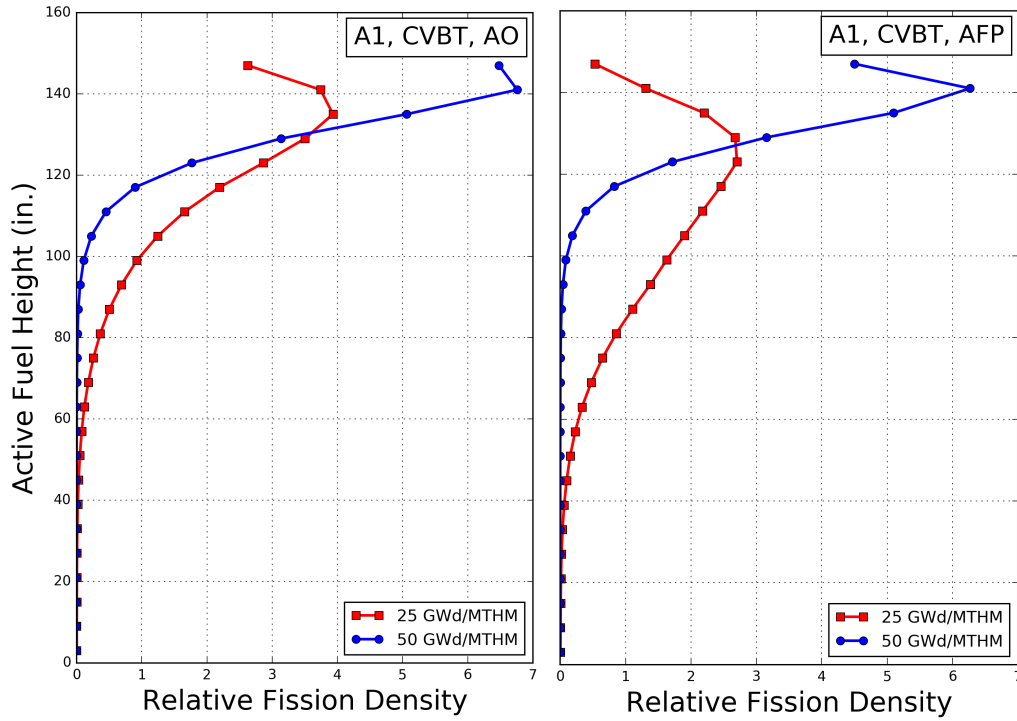
Figure 4.20. Axial fission distribution for assembly A1 CVBT case at assembly average discharge burnup values of 25 and 50 GWd/MTHM for the AO and AFP isotope sets.
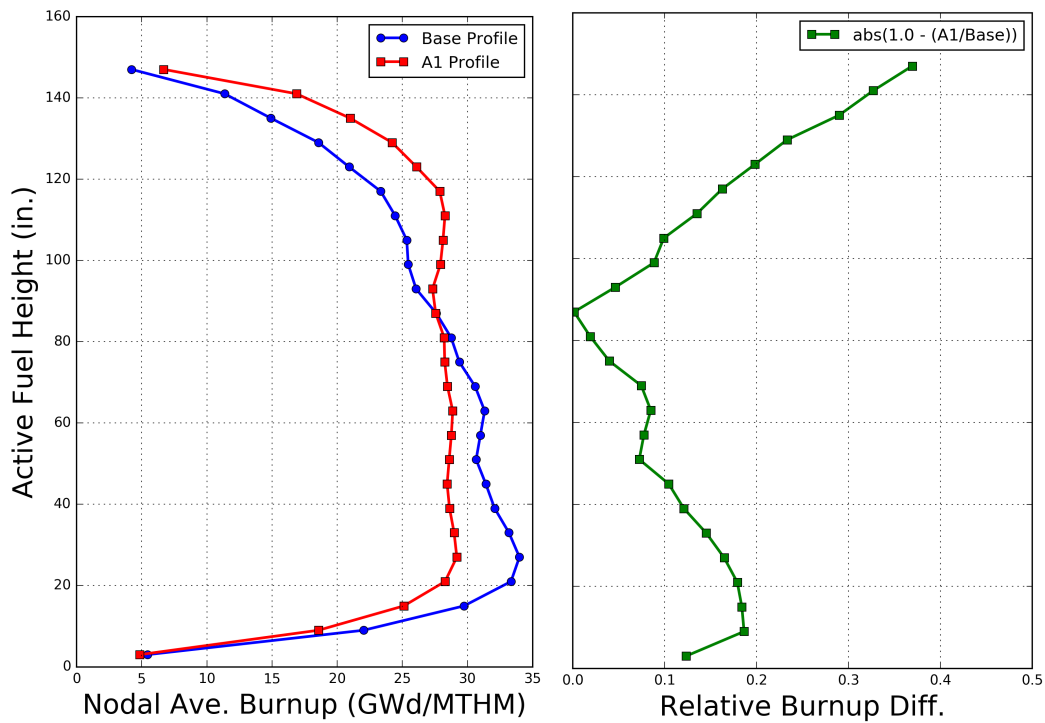
Figure 4.21. Comparison of the base burnup profile and assembly-specific burnup profile for A1.
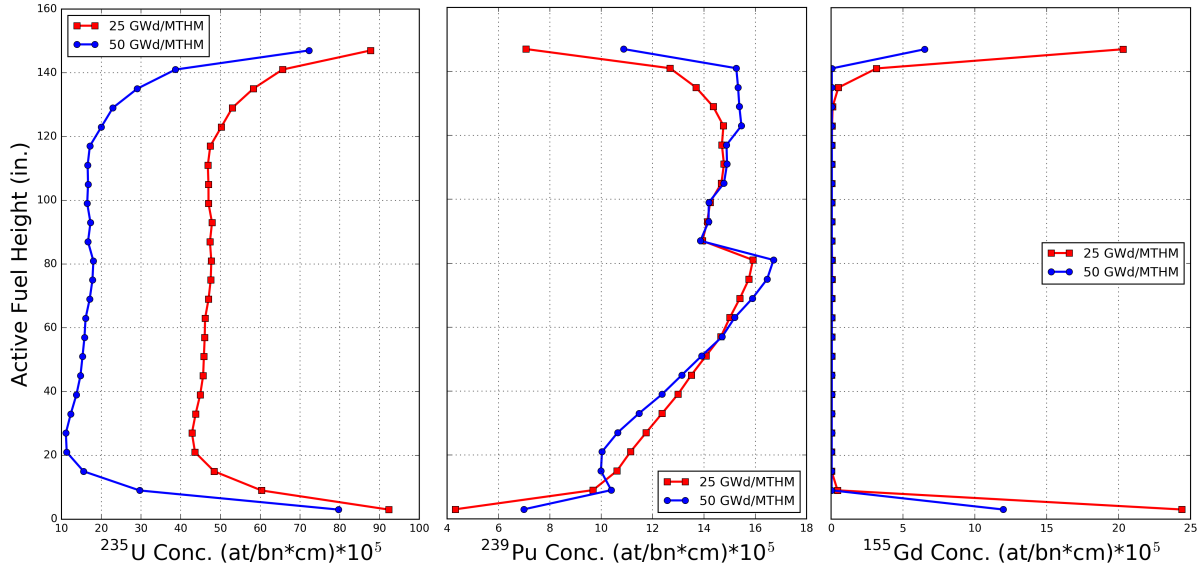
Figure 4.22. ^{235}U (left), ^{239}Pu (middle), and ^{155}Gd (right) concentration for A1 CVBT case at 25 and 50 GWd/MTHM.

Comparing the ^{235}U, ^{239}Pu, and ^{155}Gd isotopic concentrations at the two burnup values indicates why the fission density distributions are more top-peaked at 50 GWd/MTHM than at 25 GWd/MTHM, but it does not explain why there is such a significant difference when using the assembly-specific burnup profile instead of the base profile. To understand why the base burnup profile results in a higher cask k_{eff} value than the assembly-specific profiles, the ^{235}U and ^{239}Pu concentrations for A1, using the base and the assembly-specific burnup profiles, have been plotted in Figure 4.23 at the assembly-average burnup of 50 GWd/MTHM. The difference in ^{235}U remaining when using the two burnup profiles, base vs. assembly-specific, is the primary reason that the base burnup profile results in high cask reactivity when compared to the assembly-specific burnup profile. As shown in Figure 4.23, the assembly-specific burnup profile results in a slightly higher plutonium concentration at the top of the assembly than the base burnup profile, but a lower ^{235}U concentration.
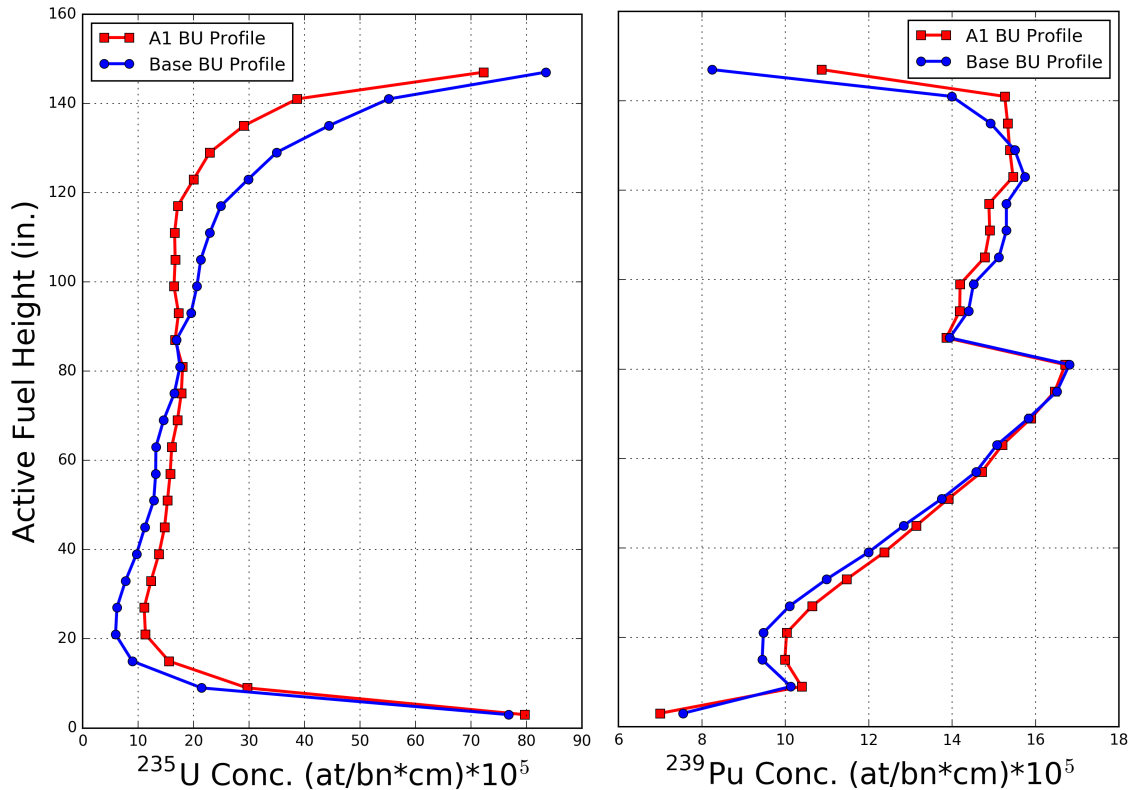
Figure 4.23. ^{235}U (left), ^{239}Pu (right), assembly A1 using the base and assembly-specific burnup profiles at 50 GWd/MTHM.

The results for A1 and A2 indicate that using assembly-specific conditions results in lower cask reactivity than the base conditions; however, the level of reactivity reduction is largely dependent on the individual fuel assembly. The reactivity reduction compared to the base conditions for A1 and A2 is relatively large, as the burnup distribution's shape, which is influenced by control blade usage, is less limiting than the base burnup profile. Namely, control blade insertion leads to higher relative burnups in the top portion of the fuel assembly, which leads to lower cask reactivity. The impact of the real control blade histories when considered separately from other parameters has a relatively small impact on cask reactivity, but when the impact on the burnup profile caused by control blade usage is considered, the overall impact on reactivity is much larger.

With respect to the addition of the burnup profile to the assembly-specific conditions, A3 is an outlier compared to A1 and A2. There is no impact to A3 with addition of the assembly-specific control blade history because A3 contains no control blade insertion. There is almost no impact to addition of the assembly-specific burnup profile for A3, whereas for A1 and A2, the addition of the assembly-specific profile has a very significant impact on cask reactivity, up to 7% Δk_{eff}. This is almost entirely caused by assembly A3 having a burnup profile nearly identical to the chosen limiting base burnup profile. However, results for A3 contain important information. First, A3 further highlights the importance of selection of the axial burnup profile. A3 also indicates that the effect of assembly-specific conditions is rather small when there is little control blade insertion and when other parameters are near limiting conditions. A3 indicates that using assembly-specific conditions still results in lower cask reactivity compared to the base conditions, but the magnitude of this reactivity reduction is small. Addition of all tested

assembly-specific conditions for A3 leads to a difference in cask reactivity of less than ~0.5% Δk_{eff} compared the base case.

The results of the assembly-specific conditions study show that the burnup profile has the largest impact on cask reactivity for the test parameters. In this particular study, unlike in NUREG/CR-7224 [4], the assemblies were not binned into similar EOC burnup bins. The limiting burnup profile, and the data from A3, were taken from a first-cycle (low-burnup) fuel assembly. Comparing assembly-specific conditions for similar discharge burnup values would lessen the effect of the assembly-specific conditions because the base burnup profile and the profiles from tested assemblies would be much more similar than they are in this study.

4.4 <u>Summary and Recommendations</u>

The impact of assembly-specific conditions was studied by performing detailed depletion calculations using assembly-specific operating conditions for control blade history, axial coolant density profile, axial burnup profile, and axial fuel temperature profile and performing follow-on fuel cask criticality calculations using the depleted fuel isotopics. The results obtained are compared to similar calculations that use limiting base conditions rather than assembly-specific conditions.

The assessments documented in this section are not comprehensive; they are based on specific assembly and cask configurations and a limited amount of available operating data. The studies herein are provided to enhance understanding of important impacts on cask reactivity rather than indicating a procedure for performing BWR BUC analysis.

The primary conclusions from the assembly-specific conditions study are that (1) individually limiting depletion conditions chosen from different fuel assemblies results in conservative cask reactivity estimates when compared to using assembly-specific data for all depletion conditions, and (2) the magnitude of the reduction in cask reactivity due to the assembly-specific conditions is highly dependent on the individual fuel assembly chosen.

The directions and magnitudes of the impacts on cask reactivity are summarized here for the correlation of the control blade, axial coolant density, axial burnup profile, and axial fuel temperature profile.

- Use of the assembly-specific burnup profile has the most significant impact on cask reactivity, which is consistent with previous findings [4]. The impact varies significantly with the considered assembly.
- Control blade insertion during operation impacts the axial shape of the axial coolant density and burnup profile. Insertion of the control blade to near full-depth tends to impact the magnitude of the axial coolant density and burnup profiles, shifting the entire curve to a lower value rather than modifying the axial shape of these profiles. Insertion of the control blade to depths of 75% or less results in significant changes to the axial power shape, leading to changes in the burnup profile. Insertion of the control blade results in a reduction in the exit coolant density of ~10% or less during the time that the control blade is inserted.
- Consistent with previous results [4], use of assembly-specific control blade history increases reactivity relative to a control blades-out assumption. The magnitude of this effect varies with the control blade history, but it is generally less than 1% Δk_{eff}.

- Addition of the assembly-specific coolant density profile to the assembly-specific control blade history reduces cask reactivity. The magnitude of this reduction is highly dependent on the assembly-specific coolant density profile.
- Simulating assembly-specific conditions results in reduced cask reactivity compared to the base case that uses a control-blades out assumption and limiting values for the coolant density and axial burnup profile. The magnitude of the reduction in cask reactivity varies for each assembly, and would also depend on the penalty taken for using the control-blades out assumption.
- The cask reactivity reduction that was observed by performing depletion calculations with assembly-specific conditions ranges from ~0.50% Δk_{eff} to more than 7% Δk_{eff}, depending on the assembly and assembly-specific conditions.

5   CONCLUSIONS

Continuing the work documented in NUREG/CR-7224 [4] on extended BWR BUC, this report documents the impacts of operating parameters used in assembly depletion calculations on spent fuel cask reactivity. The main conclusions from NUREG/CR-7224 are included in this section to provide a basis for comparing previous results and the results documented in this report. This report quantifies the individual effects of fuel temperature, bypass coolant density, power density, and operating history on cask reactivity. Additionally, it quantifies the impact that correlation of operating parameters for depletion simulations has on cask reactivity.

The conclusions herein are drawn from a relatively limited range of data because the core-follow data set used for these investigations represents a single cycle from a single reactor. Additional work should be performed to demonstrate wider applicability of the conclusions drawn here.

5.1   <u>Summary of Previous Studies</u>

Axial Coolant Density Distributions

Details of the axial coolant density profile analyses are presented in Section 4 of NUREG/CR-7224 [4]. The axial coolant density profiles used in modeling fuel depletion can have a significant impact on calculated cask k_{eff} and must be treated appropriately to ensure conservative analysis results. A summary of the impacts of axial coolant density distributions is as follows:

- A cycle-averaged coolant density is a reasonable approximation for each node of an axial coolant density profile for depletion calculations when an appropriate penalty for conservatism is applied.
- Based on the previous analysis [4], a reactivity penalty of 0.25% Δk_{eff} may be sufficient to cover potential differences between detailed and cycle average coolant density treatments in depletion calculations.
- A limiting axial coolant density profile will have low moderator densities in the top nodes of the assembly.
- Use of average coolant densities determined from consideration of multiple assemblies or multiple axial nodes will result in reactivity underprediction.
- A single coolant density value can be used conservatively in all nodes only if it is lower than the coolant densities in all nodes of the assemblies to be placed in the cask.

Control Blade Usage

The details of the control blade usage analyses are presented in Section 5 of NUREG/CR-7224 [4]. Control blade usage can have an impact on cask k_{eff} and must be treated appropriately to ensure conservative analysis results. The impact is less severe than expected as the control blades must be inserted more than 50% into the core for an extended period before they have a noticeable effect. A summary of the impacts of control blade usage is as follows:

- Control blade insertions of 50% or less for the entire depletion have virtually no impact on cask reactivity.
- Although unrealistic, the most limiting case for the AFP isotope set is 92% blade insertion for the entire depletion, which increases cask reactivity by 4.3% Δk_{eff}. The

limiting case for the AO isotope set, full control blade insertion for the entire depletion, results in a cask reactivity increase of 4.1% Δk_{eff}.

- Deeper and longer-duration control blade insertions have a much greater impact than frequent, shallower, shorter-duration insertions.
- Deep control blade insertions in the last third of life have greater impact (~1%) on reactivity than similar insertions earlier in life.
- Based on the limiting realistic histories examined, a penalty of ~0.6% to 1.2% Δk_{eff} may be sufficient to account for control blade insertion effects.

Axial Burnup Profiles

The details of the axial burnup profile analyses are presented in Section 6 of NUREG/CR-7224 [4]. Axial burnup profiles can have a significant impact on cask k_{eff} and must be treated appropriately to ensure conservative analysis results. The selection of the axial burnup profile has the largest impact on cask reactivity of any tested parameter. A summary of the impacts of the axial burnup profile is as follows:

- The range of cask k_{eff} values resulting from the profiles used in this study was as large as 7.6% Δk_{eff}.
- The limiting profile resulting from a set of available profiles is largely independent of the isotope set used. Axial blanket modeling approaches also have only a small impact on identifying the limiting profile for assemblies with 6-inch natural blankets.
- Distributed burnup profiles must be considered for extended BWR BUC. End effects of up to 12.7% Δk_{eff} were identified.
- The relative reactivity of different axial burnup profiles can be predicted reliably by considering the relative burnup in the top few nodes. Lower relative burnups lead to higher cask k_{eff} values.
- Grouping axial burnup profiles into bins based on the EOC burnup of the assembly from which the profile was taken is likely to lower calculated cask k_{eff} values at higher burnups, thereby lowering excess conservatism.

5.2 Operating Parameters

The impacts of operating parameters (fuel temperature, bypass coolant density, power density, and operating history) are relatively small compared to the impacts observed for previous studies of coolant density, control blade history, and axial burnup profile [4]. While these impacts are small, care should still be taken when modeling these conditions.

Note that the individual effects of operating parameters were determined for a single assembly's average burnup (45.2 GWd/MTHM), and therefore this study does not quantify burnup dependence on these effects. However, the established trends in cask reactivity with independent variations of the considered operating parameters are consistent with findings from other studies.

Fuel Temperature

- Cask reactivity increases with increasing fuel temperature due to increased plutonium production.
- Fuel temperature impact is ~0.10% k_{eff} and ~0.09% k_{eff} per 100 K for the AO and AFP isotope sets, respectively.
- Using the highest pellet-averaged fuel temperature for all fuel will result in a conservative cask reactivity estimate.

Bypass water density

- Cask reactivity increases with decreasing bypass water density due to increased plutonium production in these cases.
- Cask reactivity increase is less than 0.1% k_{eff} for every 1% reduction in bypass water density for both isotope sets.
- Additional data are needed to know the amount by which the bypass moderator density can change under normal operating conditions. Using bypass moderator densities higher than the saturated liquid water density should be avoided to ensure conservatism.

Specific power

- Calculations show that cask reactivity increases with increasing specific power, but the magnitude of the increase in cask reactivity is very small—on the order of the uncertainty of the calculations themselves.

Operating history

- Typical downtimes (~30 days between cycles) have a negligible impact on cask reactivity. Extended downtimes preceding an assembly's last irradiation cycle before being discharged lead to decreases in cask k_{eff} values.
- Cask reactivity is negligibly affected by the power level during assembly's last irradiation cycle relative to the lifetime average power. Cask k_{eff} slightly increases (within 2σ) with increasing power level during the last cycle for the AO set and is practically unchanged for the AFP set.

5.3 Assembly-specific conditions

The impact of the correlation of major operating conditions, coolant density profile (void profile), control blade history, and axial burnup profile, varies with each fuel assembly. Using limiting conditions for the coolant density profile, control blade history, and axial burnup profile will result in conservative cask reactivities compared to the use of assembly-specific conditions. The impacts of assembly-specific conditions were evaluated for 25 and 50 GWd/MTHM assembly average discharge burnups. The assembly-specific conditions were studied for three different assemblies. The results obtained using these three assemblies are unlikely to bound all possibilities for all reactors. Additional research is needed using multiple cycles of data from additional reactors to fully assess the impacts of assembly-specific conditions.

- Cask reactivity is reduced by using assembly-specific conditions compared to limiting conditions for the major operating conditions. The magnitude of this reactivity reduction ranges from ~0.50% Δk_{eff} to more than 7% Δk_{eff} depending on the assembly and assembly-specific conditions included.
- Using the assembly-specific burnup profile has the most significant impact on cask reactivity, which is consistent with previous findings. The impact varies significantly with the assembly selected.
- The impact of assembly-specific conditions on cask reactivity is greatest for assemblies with significant control blade insertion. Use of the control blade during operation changes the axial shape of the coolant density and burnup profile. Insertion of the control blade leads to less limiting coolant density and burnup axial profiles.
- The impacts of assembly-specific conditions on cask reactivity are greater for high discharge burnups than for low discharge burnups.

The results from previous studies [4] and the studies documented in this report all indicate that the axial burnup profile has the greatest impact on cask reactivity of any studied parameter. The significant impact to cask reactivity is due to the top-peaked axial fission distribution in BWR spent fuel casks combined with the low-burnup axial top portion of BWR fuel assemblies. The next largest impact on cask reactivity is the axial coolant density distribution. Limiting coolant density distributions have low coolant density at the top of the fuel assembly, leading to increased plutonium production. The impact of realistic control blade histories is relatively minor because few assemblies experience near full-depth control blade insertion for significant periods of irradiation. The impact of modeling assembly-specific conditions that are correlated can provide cask reactivity reductions, but the magnitude of the reduction varies significantly with each fuel assembly. The impacts of fuel temperature, bypass coolant density, power density, and operating history are all relatively small compared to the other studied parameters.

Table 5.1 provides a brief summary of the parameters studied to date (in NUREG/CR-7224 [4] and this document). Each parameter is summarized by indicating the direction and magnitude that its variation has on cask reactivity. Based on the direction and magnitude, each parameter is labeled "high", "medium", or "low" impact. Table 5.1 provides the most basic summary of each parameter—more detailed information, including burnup dependence, changes due to isotope set, etc., can be found in NUREG/CR-7224 and Sections 3 and 4 of this document.

Table 5.1.   Summary of the impact of studied parameters on cask reactivity

Parameter	Impact	Physics Basis	Direction of Variation	Magnitude	Comments
Burnup Axial Profile	High	Lower burnup is more reactive due to increased residual fissile content (^{235}U) of the fuel	Lower burnup in top axial portion of the assembly leads to higher cask k_{eff}	Variation up to 7.6% Δ k_{eff} for the tested profiles	Uniform burnup profiles are nonconservative at higher burnups, but may be considered at lower burnups
Coolant Density Axial Profile	Medium	Lower coolant density leads to harder neutron spectra, resulting in increased plutonium production	Low coolant density in the top axial portion of the assembly leads to higher cask k_{eff}	Axially uniform density corresponding to 40% void fraction yields nonconservative cask reactivity up to 10% Δ k_{eff}	Axially uniform coolant density is conservative only if chosen density is lower than all nodes in the assembly
Control Blade insertion	Medium	Control blade insertion leads to harder neutron spectra, resulting in increased plutonium production	Control blades inserted deeply into the core, late in life, for long periods of time result in high cask k_{eff}	~0.6% Δ k_{eff} increase due to control blade history for the tested assemblies	Control blade insertion less than 50% into the core has almost no impact on cask reactivity
Assembly-Specific Conditions	Medium	Variation of assembly power, due to the control blade or other factors, affects the burnup distribution, coolant density, fuel temperature, etc.	Use of assembly-specific conditions lowers cask reactivity compared to individually limiting conditions for all other parameters	Decrease in k_{eff} ranging from 0.5% to more than 7% for the tested assemblies	Insertion of the control blade tends to make other conditions (coolant density, burnup distribution) less limiting
Fuel Temperature	Low	Higher fuel temperature leads to increased ^{238}U absorption resonance widths, resulting in increased plutonium production	High fuel temperatures lead to high cask k_{eff}	~0.1% Δ k_{eff} for every 100 K increase in fuel temperature	None

Table 5.1. Continued

Parameter	Impact	Physics Basis	Direction of Variation	Magnitude	Comments
Bypass Flow Density	Low	Lower moderator density leads to harder neutron spectra, resulting in increased plutonium production	Decreased bypass flow density results in higher cask k_{eff}	~0.1% Δ k_{eff} for every 1% reduction in bypass flow density	No data available to quantify if the bypass density is lower than the saturation density during normal operation
Specific Power	Low	Increases in power density lead to less time for radioactive nuclides to decay during operation	Increasing specific power tends to increase cask k_{eff}	Very small, on the order of the calculation uncertainty	Likely a more important effect for AO isotope set than for AFP isotope set
Operating History	Low	Operating history affects the spent fuel compositions by changing the rates at which fission products and other actinides are generated or consumed	Increased power near the end of operation tends to increase cask k_{eff}, typical downtimes (~30 days) have a negligible impact on cask k_{eff}	Very small, on the order of the calculation uncertainty	None

6 REFERENCES

1. US Code of Federal Regulations Title 10, "Energy," US Nuclear Regulatory Commission, Washington, DC (2017).

2. Division of Spent Fuel Storage and Transportation, *Interim Staff Guidance – 8, Revision 3, Burnup Credit in the Criticality Safety Analyses of PWR Spent Fuel in Transportation and Storage Casks*, US Nuclear Regulatory Commission (September 26, 2012).

3. W. J. Marshall, B. J. Ade, S. M. Bowman, I. C. Gauld, G. Ilas, U. Mertyurek, and G. Radulescu, *Technical Basis for Peak Reactivity Burnup Credit for BWR Spent Nuclear Fuel in Storage and Transportation Systems*, NUREG/CR-7194 (ORNL/TM-2014/240), prepared for the US Nuclear Regulatory Commission by Oak Ridge National Laboratory, Oak Ridge, Tennessee (April 2015).

4. W. J. Marshall, B. J. Ade, S. M. Bowman, and J. S. Martinez, *Axial Moderator Density Distributions, Control Blade Usage, and Axial Burnup Distributions for Extended BWR Burnup Credit*, NUREG/CR-7224 (ORNL/TM-2015/544), prepared for the US Nuclear Regulatory Commission by Oak Ridge National Laboratory, Oak Ridge, Tennessee (August 2016).

5. D. E. Mueller, S. M. Bowman, W. J. Marshall, and J. M. Scaglione, *Review and Prioritization of Technical Issues Related to Burnup Credit for BWR Fuel*, NUREG/CR-7158 (ORNL/TM-2012/261), prepared for the US Nuclear Regulatory Commission by Oak Ridge National Laboratory, Oak Ridge, Tennessee (February 2013).

6. *SCALE: A Comprehensive Modeling and Simulation Suite for Nuclear Safety Analysis and Design,* ORNL/TM-2005/39, Version 6.2.1, Oak Ridge National Laboratory, Oak Ridge, Tenn. (August 2016). Available from Radiation Safety Information Computational Center at Oak Ridge National Laboratory as CCC-834.

7. M. D. DeHart and S. M. Bowman, "Reactor Physics Methods and Analysis Capabilities in SCALE," *Nuclear Technology*, 174(2) (May 2011): 196–213.

8. B. J. Ade, *SCALE/TRITON Primer: A Primer for Light Water Reactor Lattice Physics Calculations*, NUREG-7041 (ORNL/TM-2011/21), prepared for the US Nuclear Regulatory Commission by Oak Ridge National Laboratory, Oak Ridge, Tennessee (November 2012).

9. I. C. Gauld, G. Radulescu, G. Ilas, B. D. Murphy, M. L. Williams, and D. Wiarda, "Isotopic Depletion and Decay Methods and Analysis Capabilities in SCALE," *Nuclear Technology*, 174(2) (May 2011): 169–195.

10. I. C. Gauld, M. T. Pigni, and G. Ilas, "Validation and Testing of ENDF/B-VII Decay Data," *Nuclear Data Sheets* 120 (2014): 33–36.

11. J. M. Scaglione, D. E. Mueller, J. C. Wagner, and W. J. Marshall, *An Approach for Validating Actinide and Fission Product Burnup Credit Criticality Safety Analyses – Criticality (k_{eff}) Predictions*, NUREG/CR-7109 (ORNL/TM-2011/514), prepared for the US Nuclear Regulatory Commission by Oak Ridge National Laboratory, Oak Ridge, Tenn. (April 2012).

12. D. E. Mueller, J. M. Scaglione, J. C. Wagner, and S. M. Bowman, *Computational Benchmark for Estimated Reactivity Margin from Fission Products and Minor Actinides in BWR Burnup Credit*, NUREG/CR-7157 (ORNL/TM-2012/96), prepared for the US Nuclear Regulatory Commission by Oak Ridge National Laboratory, Oak Ridge, Tennessee (February 2013).

13. D. P. Henderson, *Summary Report of Commercial Reactor Criticality Data for LaSalle Unit 1,* B00000000-01717-5705-00138 REV 00, Civilian Radioactive Waste Management System M&O Contractor (September 1999).

14. J. C. Wagner, M. D. DeHart, and B. L. Broadhead, *Investigation of Burnup Credit Modeling Issues Associated with BWR Fuel*, ORNL/TM-1999/193, Oak Ridge National Laboratory, Oak Ridge, Tennessee (October 2000).

15. I. C. Gauld, G. Ilas, B. D. Murphy and C. F. Weber, *Validation of SCALE 5 for Decay Heat Predictions of LWR Spent Fuel*, NUREG/CR-6972, prepared for the US Nuclear Regulatory Commission by Oak Ridge National Laboratory, Oak Ridge, Tennessee (2010).

16. J. S. Martinez, B. J. Ade, S. M. Bowman, I. C. Gauld, G. Ilas, B. J. Marshall, **"**Impact of Modeling Choices on Inventory and In-Cask Criticality Calculations for Forsmark3 BWR Spent Fuel," *CD Proceedings, International Conference on Nuclear Criticality Safety ICNC'15*, Charlotte, NC, USA (September 2015).

17. US Energy Information Administration, Form GC-859, "Nuclear Fuel Data Survey" (2013).

18. J. Hu, J. L. Peterson, I. C. Gauld, and S. M. Bowman, *US Commercial Spent Nuclear Fuel Assembly Characteristics 1968–2013*, NUREG/CR (ORNL/TM-2015/619), prepared for the US Nuclear Regulatory Commission by Oak Ridge National Laboratory, Oak Ridge, Tennessee (in progress).

19. C. V. Parks, M. D. DeHart, and J. C. Wagner, *Review and Prioritization of Technical Issues Related to Burnup Credit for LWR Fuel*, NUREG/CR-6665 (ORNL/TM-1999/303), prepared for the US Nuclear Regulatory Commission by Oak Ridge National Laboratory, Oak Ridge, Tennessee (February 2000).